

**A RETROFIT ANALYSIS OF UNREINFORCED MASONRY WALLS UNDER
BLAST LOADING**

A Thesis

Presented in Partial Fulfillment of the Requirements for the

Degree of Master of Science

with a

Major in Civil Engineering

in the

College of Graduate Studies

University of Idaho

by

Chaney H. Wood

Major Professor: Ahmed Ibrahim, Ph.D., P.E.

Committee Members: Richard Nielsen, Ph.D., P.E.; Emad Kassem, Ph.D., P.E.

Department Administrator: Patricia J. S. Colberg, Ph.D., P.E.


December 2020


AUTHORIZATION TO SUBMIT THESIS

This thesis of Chaney H. Wood, submitted for the degree of Master of Science with a Major in Civil Engineering and titled "**A Retrofit Analysis of Unreinforced Masonry Walls Under Blast Loading**," has been reviewed in final form. Permission, as indicated by the signatures and dates below, is now granted to submit final copies to the College of Graduate Studies for approval.

Major Professor:  Date: 12-10-2020
Ahmed Ibrahim, Ph.D., P.E.

Committee Members:  Date: 10 Dec. 2020
Richard Nielsen, Ph.D., P.E.

 Date: 10 Dec. 2020
Emad Kassem, Ph.D., P.E.

Department Chair:  Date: 10 Dec 2020
Patricia J. S. Colberg, Ph.D., P.E.

ABSTRACT

The primary objective of this study is to find effective ways of retrofitting unreinforced concrete masonry units (CMU) walls to survive against harmful blast loading effects. The retrofit investigation considered the use of carbon fiber reinforced polymers (CFRP), Kevlar, aluminum, and steel applied to CMU and exposed to a 100-kg ANFO charge at a 15-meter standoff distance. For the experimentation, Ansys Workbench and Ansys Autodyn (finite element software) were used to model a control CMU wall and compare model simulations with the retrofit materials at varying thicknesses. The control CMU wall measured 1000 millimeters long, 2200 millimeters tall, and 200 millimeters thick. Each material was added to the control wall in 3.175-mm increments starting with 3.175 millimeters and ending with 19.05 millimeters.

The study concluded that each material made a significant contribution to decreasing the wall's overall deflection values when compared to the control. After the data collection process, a discussion was held to compare the overall percent improvement, material weight, material costs, workability, and constructability for each material selection. With all factors considered, the discussion concluded that the use of a fiber reinforced polymer would be the best retrofit option.

Keywords: Unreinforced masonry, blast loading, finite element, carbon fiber reinforced polymer, Kevlar, aluminum, steel

ACKNOWLEDGEMENTS

I would like to thank my advisor and major professor, Dr. Ahmed Ibrahim, for his support, motivation, advice, and knowledge that he has provided me during my graduate and undergraduate studies here at the University of Idaho. I am grateful for the many hours he invested in working with me through all my research and for the guidance he has provided me both inside and outside of academia. I also owe a great amount of thanks to both of my committee members, Dr. Emad Kassem and Dr. Richard Nielsen. On top of being great members of my committee, I have been honored with having them as great role models and professors during my time here.

I would like to especially thank Mahmoud Abada for his support, feedback, and knowledge that he provided throughout my thesis. His knowledge and guidance proved to be truly irreplaceable. I also could not have asked for a better classmate, colleague, and friend to work with throughout graduate research. Without him, this would not have been possible.

Lastly, I owe many thanks to the Department of Civil and Environmental Engineering as a whole. I am thankful to have spent the last five and a half years of my life working and learning from the many great faculty members. Most importantly, if it were not for the department chair, Dr. Patricia Colberg, I would not have had this great opportunity to stay and grow as a student and engineer.

DEDICATION

This work is dedicated to my father, Jason Wood, my mother, Deana Johnson, my stepmother, Cindie Wood, and my grandparents for their unconditional love, support, guidance, and encouragement that they have always given me. Without them, I would not be where I am today.

TABLE OF CONTENTS

Authorization to Submit Thesis	ii
Abstract	iii
Acknowledgements	iv
Dedication	v
Table of Contents	vi
List of Tables	ix
List of Figures	x
Chapter 1: Introduction	1
1.1 Problem Statement	1
1.2 Objective of Research.....	2
1.3 Thesis Outline.....	2
Chapter 2: Literature Review.....	3
2.1 Introduction	3
2.2 Explosives and Blast Loading	4
2.3 Concrete Masonry Unit Walls	6
2.3.1 Design Guidelines for Masonry Structures	7
2.3.2 Material Properties of Concrete Masonry Units and Components	9
2.3.3 Concrete Masonry Unit Wall Failure Modes	10
2.4 Development of Fiber Reinforced Polymer Materials	11
2.4.1 Benefits and Use of Fiber Reinforced Materials	13
2.4.2 Carbon Fiber Reinforced Polymer.....	14
2.4.3 Kevlar	15
2.5 Steel Products	16
2.6 Aluminum Products.....	17
Chapter 3: Finite Element Model.....	18

3.1 Introduction	18
3.2 Unit System	18
3.3 Dimensions and Geometry	19
3.4 Parts	20
3.5 Nodes and Elements	22
3.6 Material Models	23
3.7 Contact Interfaces.....	24
3.8 Boundary Conditions.....	25
3.9 Loading.....	27
3.10 Blast Modeling	27
3.11 Model Validation.....	31
3.12 Mesh Sensitivity Analysis	36
Chapter 4: Parametric Study	37
4.1 Introduction	37
4.2 Dimensions and Geometry	37
4.3 Parts	38
4.4 Material Selection and Material Models	39
4.4.1 Carbon Fiber Reinforced Polymer.....	40
4.4.2 Kevlar	40
4.4.3 Aluminum.....	41
4.4.4 Mild Steel	42
4.5 Contact Interfaces.....	43
4.6 Boundary Conditions.....	43
4.7 Loading.....	44
4.8 Parametric Study Results.....	44
4.8.1 CFRP Results.....	45
4.8.2 Kevlar Results	48

4.8.3 Aluminum Results	51
4.8.4 Mild Steel Results.....	54
4.8.5 Combined Summary of Results.....	57
4.8.6 Comparison with Literature.....	61
Chapter 5: Conclusions and Recommendations	63
5.1 Conclusions for Retrofitted Unreinforced CMU Walls.....	63
5.2 Recommendations for Future Work	64
References.....	65

LIST OF TABLES

Table 2-1: Material Properties of CMU [14, 16]	10
Table 2-2: Material Properties of Mortar [16, 17]	10
Table 3-1: Unit System	19
Table 3-2: CMU Wall Dimension Summary	20
Table 3-3: Concrete Masonry Model Parameters [30]	24
Table 3-4: Type-S Mortar Properties	25
Table 3-5: Air Model [31].....	28
Table 3-6: Trinitrotoluene (TNT) Model [31]	29
Table 3-7: Model Results Summary and Comparison [30]	32
Table 4-1: High Strength Prepreg CFRP Model Parameters	40
Table 4-2: Kevlar Model Parameters	41
Table 4-3: Aluminum (AL 7036) Model Parameters	41
Table 4-4: Mild Steel (4340 Alloy) Model Parameters	42
Table 4-5: Bond Stress Values for Composite Material to CMU [34]	43
Table 4-6: Peak Deflection Results for All Materials.....	58
Table 4-7: Improvement in Peak Deflection for All Materials.....	59
Table 4-8: Material Cost for CFRP, Kevlar, Aluminum, and Steel (2020 Market Values) ...	61

LIST OF FIGURES

Figure 2-3: Unreinforced CMU Wall Segment	6
Figure 2-4: Reinforced CMU Wall [15]	7
Figure 2-5: Common Masonry Unit Orientations.....	8
Figure 2-6: Various Running Bond Styles.....	8
Figure 2-7: CMU Wall Failure Modes Based on Reference [6].....	11
Figure 2-8: Unidirectional Fiber Orientation within a Polymer Matrix	12
Figure 2-9: Orthogonal Grid within a Polymer Matrix.....	12
Figure 2-10: Carbon Fiber Sheet before Matrix Application.....	15
Figure 3-1: Abou-Zeid et al. Experimental Setup Rendition.....	20
Figure 3-2: a) Standard Two-cell CMU, b) Single-cell CMU	21
Figure 3-3: Steel Clamp	21
Figure 3-4: Isometric View (left) and Side View (right)	22
Figure 3-5: Isometric View with Wall Meshing.....	23
Figure 3-6: Steel Clamps with Applied Boundary Conditions	26
Figure 3-7: CMU Wall with Applied Boundary Conditions	27
Figure 3-8: 2-D Wedge Atmosphere Element	28
Figure 3-9: 2-D Wedge Element with Displayed Boundary Conditions	29
Figure 3-10: 2-D Wedge Element Containing TNT Charge and Atmosphere	30
Figure 3-11: Complete Combined Model	31
Figure 3-12: Ansys Autodyn Data (100 kg at 15 m)	33
Figure 3-13: CMU Wall Model Post Blast	34
Figure 3-14: 4-kg ANFO Charge at 10 Meters.....	35
Figure 3-15: 10-kg ANFO Charge at 10 Meters.....	35
Figure 3-16: 19.05 mm Mesh (left) and 6.35-mm Mesh (right)	36

Figure 4-1: Meshed Retrofit Material (left) and New Composite CMU Wall (right)	39
Figure 4-2: Material Addition with Defined Boundary Conditions.....	44
Figure 4-3: Ansys Autodyn Model Displacement-Time History Results for CFRP	46
Figure 4-4: 3.175-mm Thick CFRP Retrofit During Peak Displacement	47
Figure 4-5: Peak Deflection and Percent Improvement in Deflection for CFRP	48
Figure 4-6: Ansys Autodyn Model Displacement-Time History Results for Kevlar	49
Figure 4-7: 3.175-mm Thick Kevlar Retrofit During Peak Displacement	50
Figure 4-8: Peak Deflection and Percent Improvement in Deflection for Kevlar	51
Figure 4-9: Ansys Autodyn Model Displacement-Time History Results for Aluminum.....	52
Figure 4-10: 3.175-mm Thick Aluminum Retrofit During Peak Displacement.....	53
Figure 4-11: Peak Deflection and Percent Improvement in Deflection for Aluminum.....	54
Figure 4-12: Ansys Autodyn Model Displacement-Time History Results for Mild Steel	55
Figure 4-13: 3.175-mm Thick Steel Retrofit During Peak Displacement	56
Figure 4-14: Peak Deflection and Percent Improvement in Deflection for Mild Steel	56
Figure 4-15: Peak Deflection Results for All Materials	58
Figure 4-16: Improvement in Peak Deflection for All Materials	59
Figure 4-17: Weight per Percent Improvement in Deflection	60

CHAPTER 1: INTRODUCTION

1.1 PROBLEM STATEMENT

Today, we have a continually growing concern for the human lives being affected by cruel acts of terrorism. These acts of terrorism have reached across the globe and often include the use of explosive material to achieve high levels of destruction. For a single act alone, the use of these explosive materials has shown to be devastating and detrimental to innocent lives. Modern examples of these horrible events include the Oklahoma City bombing (1995), Norway attacks (2011), and the Boston Marathon bombing (2013) [1, 2, 3]. Among these intentional blasts, there have also been rare occasions of unintentional detonation of explosive material. The most recent example being the devastating 2020 Beirut, Lebanon explosion [4]. No matter the source of explosion, we need ways to protect innocent lives as well as our essential facilities. One method to do so is by simply improving or retrofitting our current structures to withstand these extreme and unfortunate scenarios.

Masonry structures are well-known across the globe and masonry is still one of the most popular construction materials [5]. Masonry buildings constructed without steel reinforcing are extremely vulnerable to any form of high-intensity lateral loading. This vulnerability of unreinforced masonry has created an increased concern regarding intentional blast loading. With so many masonry structures already existing in many parts of the world, there must be ways to improve existing structures and prevent the harm or loss of life of those residing within them.

With the continued improvements in material science, there is an increasing amount of engineered high strength and lightweight materials. A few well-known materials include carbon fiber reinforced polymers (CFRP), glass fiber reinforced polymers (GFRP), and aramid fiber reinforced polymers (AFRP). The ease of application and high strength values provided from these reinforcing fibers have shown to be useful in the retrofit of many structural elements, including concrete columns, slabs, decks, and masonry. Although, much of the research directed at masonry structures is still being investigated and may become one of the best alternatives for protecting our vulnerable unreinforced masonry structures against blast loading.

1.2 OBJECTIVE OF RESEARCH

The primary objective of this study is to find effective ways of retrofitting unreinforced concrete masonry unit (CMU) walls to survive against harmful blast loading effects. This can be achieved by creating a finite element model of an unreinforced masonry wall that is validated through existing experimental data. After the creation of the model, different retrofit options for material (CFRP, Kevlar, aluminum, and steel) were added into the finite element model with its performance investigated under blast loading. The peak deflections from the model analysis can then be compared to the original control deflections.

A secondary objective of this study is to form conclusions on the best method for general use between the four materials. This includes the consideration of peak wall deflection, constructability, workability, cost, and material weights.

1.3 THESIS OUTLINE

The thesis is divided into four chapters (Chapters 2-5) that present an analysis of blast loading on a retrofitted unreinforced masonry wall using commercial finite element software.

Chapter 2: “LITERATURE REVIEW”: This chapter summarizes relevant and current research that has been performed on masonry structures for against blast loading and the use of fiber reinforced polymers.

Chapter 3: “FINITE ELEMENT MODEL”: This chapter covers the complete process of the finite element model creation and its validation.

Chapter 4: “PARAMETRIC STUDY”: This chapter describes the modified model creation and explains parameters that were investigated during the experiment. Furthermore, this chapter explains the results of each model and how it compared to the control experiment.

Chapter 5: “CONCLUSIONS AND RECOMMENDATIONS”: This chapter presents the conclusions that were composed from the results of the parametric study (Chapter 4) in addition to providing recommendations for future research.

CHAPTER 2: LITERATURE REVIEW

2.1 INTRODUCTION

Masonry structures have been used around the world for centuries and are still one of the most popular construction materials [5]. With the growing concern of terrorism across the globe, there is also a growing concern of how these structures will react to extreme loading conditions such as blast loading [6]. Specifically, masonry buildings comprised of unreinforced masonry units (CMU), also known as cinderblocks, are of highest concern due to their low out-of-plane bending strength and their high vulnerability to fragmentation [7, 8, 9]. Their abundance of joints also allows many possible failure planes to occur in any loading event [8].

So far, relatively little research has been conducted on the mitigation of harmful blast loading effects on unreinforced CMU walls and how these walls react to blast loads [9]. For construction in many parts of the United States, new buildings must be designed using reinforced CMU rather than unreinforced [10]. Therefore, most of the research that has been done was for the retrofitting of unreinforced masonry walls with various blast resistant materials to withstand intentional or unintentional explosion events [11]. These blast resistance materials are most commonly different types of fiber reinforced polymers (FRP), such as: carbon fiber reinforced polymer (CFRP), glass fiber reinforced polymer (GFRP), aramid fiber reinforced polymer (AFRP), and even aramid/glass (A/G) hybrid polymers [7]. When compared to other methods, P.A. Buchan [7] states that FRP is a desired method of strengthening due to its high strength to weight ratio and its ability to resist corrosion. FRPs are also easily installed and require minimal intrusion on existing interior spaces as opposed to other retrofitting options. There has also been new research on the use of various polymer sprays, walls covered in steel plates, or walls lined with steel bracing [7]. These other forms of retrofitting, such as the installation of steel bracing, can be costly, detrimental to the structure's aesthetics, and increase wall thickness significantly, [8]. These three factors are vital considerations because people will not want to occupy a space that they feel is in danger, and stakeholders do not want their existing workspace decreased while also paying high retrofit prices.

Various methods have been used that do not require the alteration or modification of existing structural elements. One common example would be increasing the potential standoff distance through the installation of bollards and fencing. This method helps to keep vehicles and people that could potentially carry a bomb to be further away from the structure's surface [11]. Even though these alternative methods help to reduce threat, these methods cannot be completely relied on. Most buildings that are in harm's way of blasting are in densely populated urban areas, which means that creating proper standoff distances is not always a feasible option [11].

When looking at the protection of unreinforced CMU walls, the use CFRP and AFRP has been minorly investigated. The research of using CFRP has been primarily focused on the retrofitting of beams, columns, and slabs through experimental and theoretical approaches [7]. Research using AFRP has been invested even less than CFRP and has had focuses in improving wall strength. The only mention in the *ASCE Blast Protection of Buildings* manual [4] regarding FRP materials and masonry is that it shall be used only as a reinforcement in the tension face of masonry walls.

2.2 EXPLOSIVES AND BLAST LOADING

Before beginning the design process and modeling of explosives, it is important to understand the uniqueness of blast loads when compared to typical dynamic loads. Explosions can produce pressures that reach several orders of magnitude beyond typical dynamic loads while also having an impact that lasts only tenths of a second [6]. The two primary factors that control the magnitude of these loads are the explosive's charge weight and standoff distance (i.e., the distance from the surface to source of explosion) [12].

The actual pressure behavior over time on an object is complex with many pressure change variations over time. An example of a true pressure-time history can be seen in Figure 3 of reference [6]. Due to this complexity, the American Society of Civil Engineers (ASCE) and the Structural Engineering Institute (SEI) has created an idealized pressure-time history for both normal and oblique reflection [12]. This process is laid out within the *Blast Protection of Buildings* (ASCE/SEI 59-11) manual, as well as the entire design process for interior and exterior explosions and directly and indirectly loaded surfaces [12].

There are certain circumstances that must be met to apply the ASCE/SEI 59-11 design procedure. These circumstances differ depending on whether it is an interior or exterior explosion. It is important to categorize what type of blast is needed to be designed for, which are usually grouped as intentional (e.g., acts of terrorism) or unintentional (e.g., ignition of stored combustibles). If all the circumstances in the ASCE/SEI 59-11 are met, then the procedures laid out in Chapter 4 of the manual shall apply.

Today, explosives are composed of many different products that all produce different levels of pressure with the same charge weights. This variation of products creates difficulty and complexity in creating standardized design values that may predict other explosion scenarios. To minimize complexity, the *Blast Protection of Buildings* manual [12, Table 4-1] has converted fifty explosive values into equivalent trinitrotoluene (TNT) masses, W_e , and created a scaled distance, Z , using both equivalent masses and actual standoff distance, R (Equation I).

$$Z = \frac{R}{W_e^{1/3}} \quad (\text{Equation I})$$

When the values for two charge and stand-off distance scenarios match, this indicates that their blast waves are equal. The use of these scaling laws to explosion data has been proven to be an acceptable method of converting known explosion test data to similar larger or smaller cases [6]. The condensing of all these blast load factors into simplified transferable values helps to combat the difficulty in conducting actual blast load tests. Conducting true experimental blast loading tests can be costly, dangerous, require significant amounts of space, and require federal or local government approval which can be a long and complex process. Therefore, by using these simplified models and scaled values from the ASCE/SEI 59-11, it helps bypass many of the experimental difficulties while producing theoretically identical results. With the advancements in modern technology, there is also a continually growing industry of finite element software that can be used to model and experiment with different explosives over a wide range of materials.

2.3 CONCRETE MASONRY UNIT WALLS

Concrete masonry unit (CMU) walls are typically comprised of concrete blocks, grout, and mortar [13, 14]. Depending on whether the wall is unreinforced or reinforced, CMU walls may also have reinforcing steel. As defined by the Federal Emergency Management Agency (FEMA), unreinforced masonry walls are walls that, “do not have reinforcing steel bars placed vertically in the hollow cells or horizontally between the courses” [10]. In other words, unreinforced masonry considers the tensile strength of the masonry units and mortar and does not consider reinforcing steel tensile strength [14]. Shown in Figure 2-1 is a typical example of an unreinforced CMU wall. It is important to notice that in this figure the only three components are concrete masonry units, grout, and mortar between the joints. Even though grout can be used in unreinforced masonry design, it is not a design requirement and may be omitted.

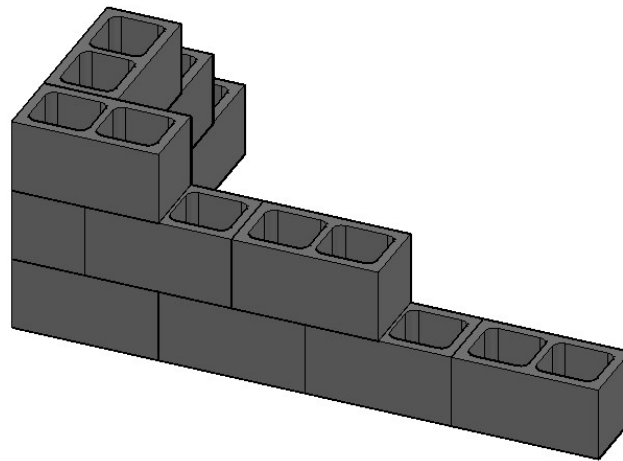


Figure 2-1: Unreinforced CMU Wall Segment

As stated previously, the only difference to a reinforced masonry wall is the implementation of reinforcing steel in the vertical and horizontal directions. The use of steel reinforcement is shown below in Figure 2-2.

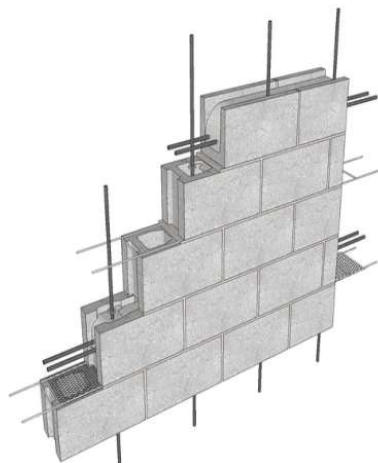


Figure 2-2: Reinforced CMU Wall [15, <https://www.imiweb.org/02-410-012-horizontal-joint-reinforcement-tolerance/>]

2.3.1 Design Guidelines for Masonry Structures

In the United States, all building load calculations are dictated by either the *International Building Code* (IBC) or the *Minimum Design Loads and Associated Criteria for Building and Other Structures* (ASCE 7). Both codes apply to masonry structures and dictate the design and calculation of gravity and lateral loads. Beyond calculating loads, the *Building Code Requirements for Masonry Structures and Commentary* (TMS 402-13) specifically dictates how masonry structures are structurally designed using two different design methods. These methods are the strength design method and the allowable-stress design method [16]. Masonry structures also need to have a defined masonry unit type, running bond pattern, grout use, and mortar type specification.

Masonry units have been grouped into a wide range of classifications, which include unfired clay masonry units, fired clay masonry units, concrete masonry units, and other miscellaneous masonry units [16]. All these types are then described using nominal dimensions of thickness, height, and length measurements. These nominal dimensions assume half a joint thickness (10 mm) on each side, making the actual size of the units 10-mm smaller than the labeled dimensions. For a typical concrete masonry unit, the nominal dimensions are 200-mm thick by 200-mm high by 400-mm long [16]. The orientation of these masonry units has many possibilities and depends on the design choice. However, there are typical orientations that are followed in masonry construction. For example, the stretcher orientation is the most common,

while the soldier orientation is most used in wall openings (e.g., windows and doors) (Figure 2-3) [16].

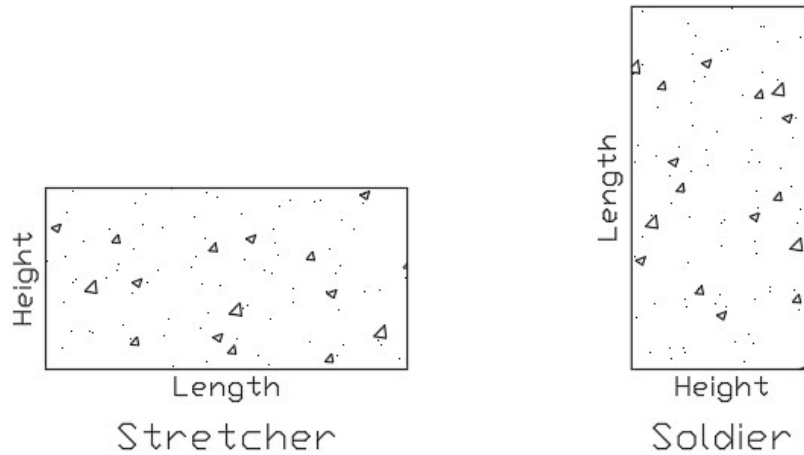


Figure 2-3: Common Masonry Unit Orientations

During the construction of unreinforced masonry walls, it is important that the masonry units be placed in running bond. According to the TMS 402-13, the running bond is “the placement of masonry units such that the head joints in successive courses are horizontally offset at least one-quarter the unit length” [14]. Figure 2-4 shows examples of the proper typical running bond construction. If a wall is not laid in running bond (i.e., stack bond), then the wall must have horizontal reinforcement throughout. The Flemish bond is also given to show one of the many other possible running bond layouts in masonry walls [16].

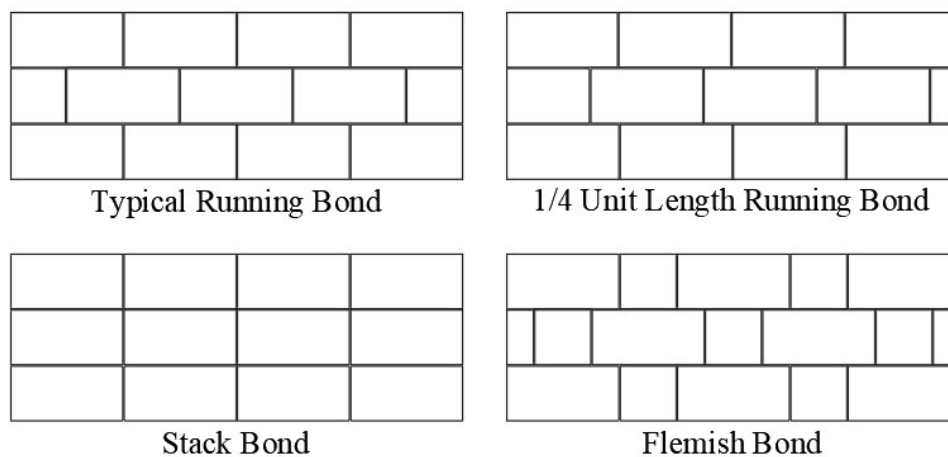


Figure 2-4: Various Running Bond Styles

Mortar is used to create the bond that holds each masonry unit together and create the running bond. The specification of the mortar and its material properties is controlled under ASTM

C270 and listed under three possible cementitious systems: cement-lime mortar, masonry-cement mortar, and mortar-cement mortar [16]. Once one of these three systems is selected, there are four mortar types to select (listed from highest strength to least): M, S, N, and O [16]. The selection of the cementitious system and mortar type is all dependent on the requirements of the system being designed for or by the designer and user preferences. In *Masonry Structural Design*, it states the type S mortar is known to be a “good all-purpose mortar” and that the selection of a cementitious system has been historically controversial. This controversy has come from the individual preferences of balancing material strength with workability. Cement-lime mortar has the major benefit of providing a high tensile bond strength, but with the downside of workability. Masonry-cement mortar has a weaker tensile bond strength, but with greater workability. This is where the selection of each may depend solely on user preferences rather than design.

Masonry grout is a mixture of Portland cement, sand, and often, pea gravel. Grout is used in masonry to surround and anchor reinforcement by filling in some, or all, of the hollow units. Grout can also be used as fill between wythes [16]. Grout’s most important property is its compressive strength, which differs with the use of concrete or clay masonry. For concrete masonry, the compressive strength of grout is controlled by the compressive strength of the masonry. The grout compressive strength may not exceed the compressive strength of the concrete masonry unit, while also remaining maintaining a minimum of 13.79 MPa and be no greater than 34.5 MPa [14, 16]. The use of grout to completely fill CMUs is optional in unreinforced masonry design because it does not have reinforcement bars.

2.3.2 Material Properties of Concrete Masonry Units and Components

The TMS 402-13 and the ASTM standards give all needed material properties for all components of masonry design. The tables showing material properties for typical CMUs and mortar are listed below in Table 2-1 and Table 2-2, respectively.

Table 2-1: Material Properties of CMU [14, 16]

Property	Value	Units
Compressive Strength (f_m)	10.34 to 20.68	MPa
Tensile Strength	$10\% \times f_m$	-
Elastic Modulus (E_m)	6.9 to 20.68	GPa
Modulus of Rigidity	$0.4 \times E_m$	-

Table 2-2: Material Properties of Mortar [16, 17]

Property	Value	Units
Compressive Strength (Type S)	12.41 (for masonry-cement)	MPa
Tensile Strength	0.52	MPa
Shear Strength	0.93	MPa
Min. Failure Strain	0.001	-
Tensile Bond Strength	≤ 241 (for masonry-cement mortar)	kPa

2.3.3 Concrete Masonry Unit Wall Failure Modes

Flexural, diagonal shear, direct shear, and breaching are the four main failure mode types for masonry walls, with flexural failure being the most desirable in blast load scenarios. Flexural failure is when the wall deflects out of plane and fails in bending before masonry units are crushed (Figure 2-5). This mode is most desirable because it provides ductility, safety from debris, and prevents wall fragmentation [6]. To achieve flexural failure, it often helps to add reinforcement material to the wall to prevent any shearing or crushing before deflection [6].

In diagonal shear, failure occurs when the diagonal tension resistance of the masonry fails before flexural failure (Figure 2-5). This failure mode is brittle and can create fragmentation that will harm anyone within or near the structure; therefore, it should be avoided when designing against blast loads. Common methods to decrease the chance of diagonal shear failure include increasing wall thickness, grouting masonry cells, and adding in steel reinforcement [6].

Direct shear is another brittle failure mode that occurs when the mortared joints fail to transfer the shear stress to the surrounding masonry units (Figure 2-5). This happens often when a substantial load (e.g., explosion) is set in very close proximity to the masonry wall [6]. Like diagonal shear, this mode can create fragmentation and debris which should be avoided in blast load design. Unfortunately, one of the only ways to help prevent direct shear from occurring is to increase the standoff distance from the detonation point [6].

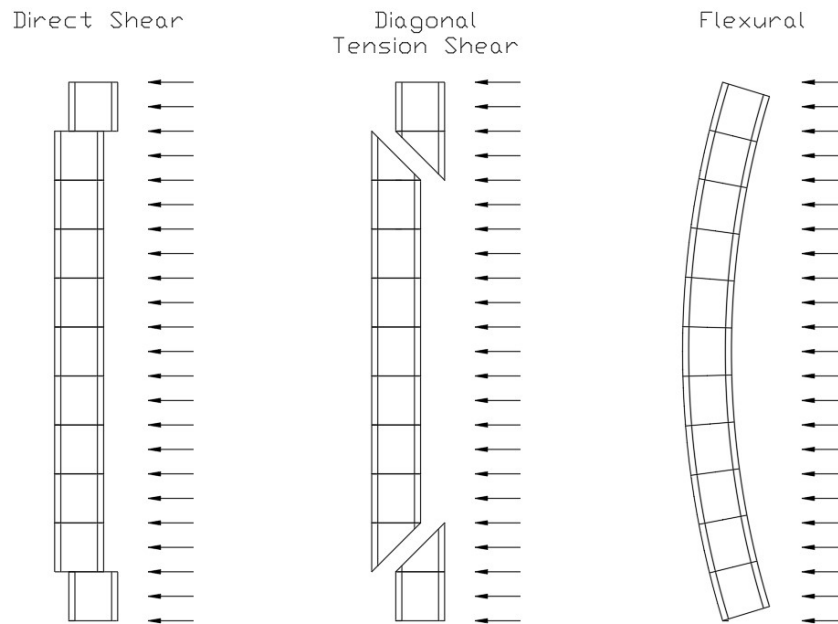


Figure 2-5: CMU Wall Failure Modes Based on Reference [6]

The last failure mode, as well as most destructive, is breaching. Breaching occurs when explosives are applied directly to the surface of a structure (contact detonation) [6]. Breaching obliterates the masonry units which causes extreme fragmentation and complete failure. Even in the case that a breaching charge does not go through the entirety of the wall, fragmentation and spall will generally take place on the tensile side of the wall [6].

2.4 DEVELOPMENT OF FIBER REINFORCED POLYMER MATERIALS

Fiber reinforced polymer (FRP) materials are materials that are composed of high strength fibers bound together within a polymer matrix and shaped as sheets, fabrics, or plates. This polymer matrix allows the fibers to act as a single unit, transferring loads between all fibers, while also providing protection of the reinforcing material [18]. These FRP materials vary in strength depending on the fiber and polymer matrix composition and fiber orientation.

Typically, these fibers are manufactured to be orientated as unidirectional (Figure 2-6) or as orthogonal grids (Figure 2-7) [19].

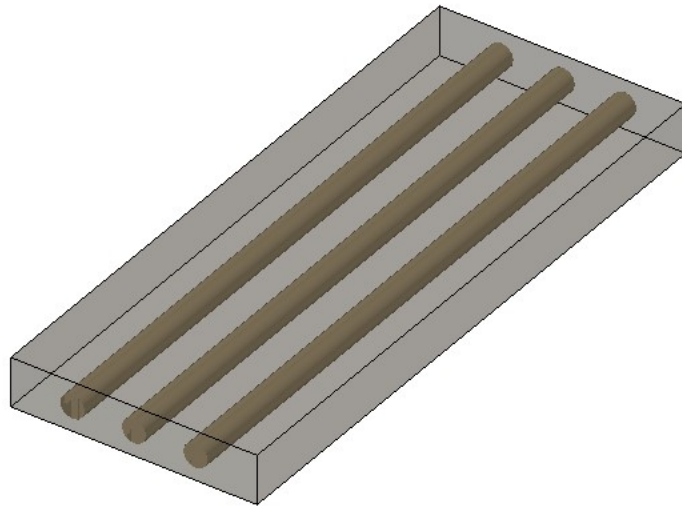


Figure 2-6: Unidirectional Fiber Orientation within a Polymer Matrix

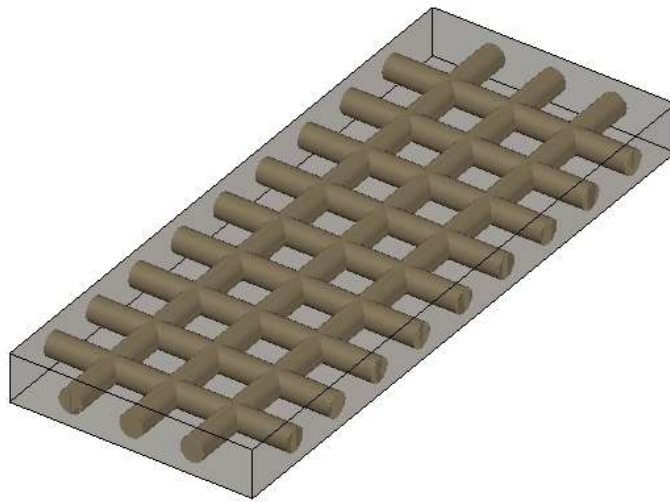


Figure 2-7: Orthogonal Grid within a Polymer Matrix

Since the 1950s, FRP materials have been utilized in the aerospace, aviation, automotive, maritime, and sports equipment manufacturing industries [20]. For use in building construction and design in the United States, FRP materials began being used merely 30 years ago [18, 19]. Existing research has focused on using FRP materials to strengthen bending strength capacities of concrete beams. Grace et al. [21] and J.Q. Ye [22] each performed tests on reinforced concrete beams bonded to FRP materials (fabrics, sheets, and plates) that were then subjected to loading. Both studies concluded that these materials do allow beams to

achieve higher ultimate load values, but at the cost of beam ductility. Unfortunately, many of the existing studies of FRP reinforced structures have not thoroughly investigated these structures under any extreme dynamic loads (i.e., blast loads) [7]. Comparing the results of a FRP reinforced structure under dynamic loads versus static loads is important because the FRP material responds differently. The complexity, cost, and the likelihood of a structure receiving explosive loads, is most likely why many researchers have focused on static load cases. Oesterle et al. [13] bypassed these issues by using blast wave generators to replicate the impact of blasts on a CMU wall with CFRP. They concluded that the CFRP retrofit does in fact improve the out-of-plane bending strength of the CMU wall and help prevent CMU walls from total collapse.

2.4.1 Benefits and Use of Fiber Reinforced Materials

There are many ways to solve problems and create structures to withstand any situation, but with each solution comes with a different price that an owner must pay. This leads to cost being one of the most influential parameters of design and construction. As a composite material, FRP has a high strength to weight ratio as opposed to other common reinforcing material (i.e., rebar) and is relatively thin in layer thickness. These two factors mean that the application of FRP to an existing structure can be done quickly and easily without using excessive resources [7]. It also allows for the smallest decrease in a building's usable square footage when compared to other structural solutions, such as the application of vertical steel bracing and installation of steel plating [7, 18]. Using the FRP material provides a discreet option that helps maintain and preserve structural aesthetics [8].

Along with its relatively low cost, FRP has many other favorable mechanical properties that encourage its use in the design and retrofitting of structures. Compared to typical steel reinforcing, these fibers provide extremely high ultimate strength values and lower modulus of elasticity. When a structural member requires an increase in flexural capacity, the application of an FRP material to the member's tensile side can provide a significant increase in flexural (bending) strength [8]. In some cases, this capacity has been increased nearly 40% [23]. One major downside to using a typical steel reinforcement method is steel's vulnerability to corrosion. To prevent this corrosion, steel reinforcement is often imbedded in concrete or coated in an epoxy to protect it. Unlike steel, FRPs are excellent in their resistance to corrosion,

giving them a wide range of application environments [7, 18]. This means that the FRP can potentially improve a member's flexural capacity more easily and efficiently over time.

A major concern in blasts lies in the potential harm to human life through fragmentation. As seen in section 2.3.3, breaching failure is the most destructive and causes the most spall and fragmentation. By permanently applying a laminate material to a wall's surface, it can prevent the spall and fragmentation from entering the building, ultimately removing this threat to human lives [6, 8].

With FRP materials still in testing and development, there are still some issues that need to be considered before use. The major concern using prefabricated FRP elements is their stiffness. This stiffness limits their use to straight structural members. This can be remediated with the use of unidirectional or orthogonal FRP sheets. FRP sheets have the capability to wrap around structural members while still providing increased strength. With both forms, it is important that the polymer be correctly applied to a structure's surface. If not applied correctly, the FRP bond will fail which will lead into an FRP-structure system failure and will ultimately provide no structural support [18].

2.4.2 Carbon Fiber Reinforced Polymer

Carbon fiber reinforced polymers (CFRP) are the most common FRP systems due to their high tensile strength, stiffness, and durability when compared to other polymer type properties [18]. CFRP also has the greatest range in material strength and is the strongest option to resist creep-rupture [19, 23]. Carbon fibers are produced and categorized into five major categories depending on their modulus of elasticity; these include: low modulus, standard modulus, intermediate modulus, high modulus, and ultra-high modulus [23]. The material properties of a CFRP material are highly dependent on the manufacturer and the carbon fiber products they offer. Manufacturers typically create the products for specific uses that are common among an array of industries. Therefore, there is no specific data set that dictates all CFRP material.

Manufacturers also produce products that vary in method of application. Some CFRP products require that the carbon fiber and the matrix be applied at the same time. This requires on-site mixing of resins that are then applied to the carbon fiber during material placement. Another option given by manufacturers is prepreg CFRP. Prepreg CFRP is a carbon fiber reinforcement

that has been pre-impregnated with a resin (typically an epoxy resin) that allows the user to apply the CFRP directly to the surface of the desired material without any further resin or hardener application [24].

Shown below in Figure 2-8 is a carbon fiber sheet before being applied to a surface using an epoxy or other polymer matrices. It is important to note the carbon fiber has much more flexibility before is embedded into a matrix. When a matrix, such as epoxy, is applied in combination with the carbon fiber, it gains much more rigidity and becomes composite with the matrix and material that it has bonded to.

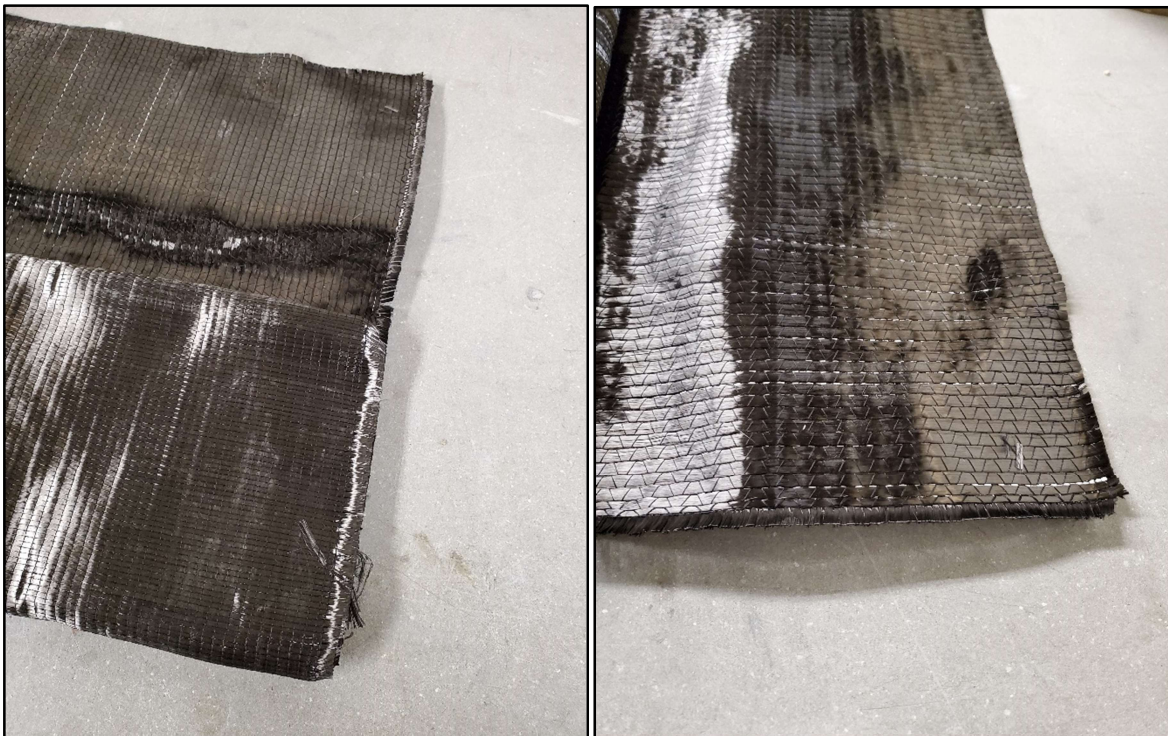


Figure 2-8: Carbon Fiber Sheet before Matrix Application

2.4.3 Kevlar

Kevlar, a man-made para-aramid synthetic fiber of the DuPont Company, is another commonly known high strength fiber. It is used because of its favorable high strength to weight ratio, high modulus, toughness, and thermal stability [25]. These traits have given it a wide range of uses among industries including automotive, mass transportation, fiber optics, ropes and cables, personal protection, and the military. Kevlar has seen its greatest and most well-known use as a personal protection material creating body armor, jackets, vests, and helmets for

military agencies worldwide [25]. When it comes to use outside of the military and use in the structural industry, it is not nearly as common and still developing. There have been few tests performed using Kevlar for this purpose because of this military dominance [7]. Some research has been performed to see if aramid fibers, and specifically Kevlar, can be used in structural applications. A test by Oesterle et al. showed that the use of aramid material, specifically Kevlar, can be used to decrease the deflection of a CMU wall and increase its bending capacity [13].

By itself, Kevlar is a highly flexible material that can be rolled and molded to fit a particular shape. When mixed and bound within a matrix, this material acts like carbon fiber and creates a bond with another material. This solidifies the Kevlar and makes it more rigid, creating a composite member with the material it has been bonded to and modifying its overall behavior.

Again, like carbon fiber, the Kevlar is manufactured to suit the needs of a specific industry or application. Therefore, DuPont has Kevlar products with a variety of material properties and does not have one specific data set to be used [26].

2.5 STEEL PRODUCTS

The production and manufacturing of steel dates to the mid-1800s [5]. Since then when we have seen many developments in steel in the form of different alloys. These alloys, as many as 250,000 different types, are modified versions of steel that allow it to be utilized across a wide range of industries and applications [5]. Steel products that are used within the construction industry have been broken down into more specific categories, that in themselves have different material strengths. These products include, but are not limited to, structural steel, cold-formed steel, fastening components, and reinforcing steel [5].

Some structural applications use steel over other materials due to steel's high strength, durability, and versatility [27]. As a primary structural element, steel is applied in the form of beams, columns, trusses, bridge girders, frames, and bracings [5]. Even when these structural elements are not used as the primary framework, steel is found in the form of high strength bolts between connections or as the reinforcing steel embedded in concrete. Steel's disadvantage is that it is both dense and is vulnerable to corrosion [5].

With respect to masonry structures, steel is used a main form of reinforcement. When used as reinforcement for concrete masonry walls, it increases the wall strength, ductility, load resistance, and resistance to shrinkage cracking [28]. The steel is often laid vertically and horizontally within masonry units and between wythes to achieve these strength improvements.

2.6 ALUMINUM PRODUCTS

Aluminum is the third most abundant element and the most abundant metal on earth [5, 29]. Architectural, transportation, consumer goods, and electrical industries have all taken advantage of aluminum's abundance and desirable material properties. Using aluminum provides a system with a material that is durable, resistant to corrosion, ductile, recyclable, conductive, and has a high strength to weight ratio [29]. Even though this material has many desirable characteristics, its use is limited for structural engineering aspects because of steel's superiority [5]. When used within structural applications, aluminum is most often used purely for architectural elements.

With respect to masonry and aluminum structural applications, this combination is nonexistent.

CHAPTER 3: FINITE ELEMENT MODEL

3.1 INTRODUCTION

Creating, analyzing, and using a finite element model (FEM) is an extended process that combines known material properties, boundary conditions, and known mathematical behavior, to model real-world situations that can then be used to predict the situation's outcome. The use of a finite element model can be valuable in many applications because it can allow for repetitive testing without exhausting valuable resources. For explosive blast analysis, it is also a way to conduct research while removing the potential blast related dangers to both researchers and to the public. Before any model can be used to predict data or a series of events, it must go through the process of completion and validation to ensure accuracy and reliability in results.

All aspects of your desired scenario must be considered and input when creating a model. This combination of variables takes time and careful observation to ensure that all variables are acting appropriately. These inputs and variables include: a global unit system, dimensions and geometry, individual parts, nodes, elements, material properties, material models, contact interfaces, boundary conditions, and loads. After an initial model is formed using the known variables, the model must pass through a validation process. This validation can be achieved through the comparison of known experimental data or mathematical processes.

The experiment performed by Abou-Zeid et al. [30] at McMaster University was used for the creation and validation of a complete finite element model to be used in analysis. This experiment used 12 unreinforced CMU walls and exposed them to various explosive charge weights and standoff distances. For the blast source, all the tests used Ammonium Nitrate Fuel Oil (ANFO) detonated at ground level. Pressure transducers and LVDTs were used to record the reflective blast pressures and the peak displacement of the CMU structure. A model was created and validated within Ansys Autodyn (finite element software) using the material properties and recorded data from Abou-Zeid et al.

3.2 UNIT SYSTEM

The unit system selected for both Ansys Workbench and Autodyn is show in Table 3-1.

Table 3-1: Unit System

Measurement	Unit
Length	Millimeter
Time	Milliseconds
Mass	Milligram

3.3 DIMENSIONS AND GEOMETRY

The details of Abou-Zeid et al.'s CMU experimental walls were followed in the creation of the wall's geometry. The wall used concrete masonry blocks with Type-S mortar as the bonding agent between the block joints. Each CMU used was made of standard two-cell concrete blocks with nominal dimensions of 400 mm wide, 200 mm tall, and 200 mm thick. For the portions of wall that required half a block in length, the block was trimmed to single-cell block nominal dimensions of 200 mm wide, 200 mm tall, and 200mm thick. The entire CMU wall was 2.5 blocks wide, 11 courses tall, and a single wythe thick (Table 3-2). The mortar thickness in the experimental wall by Abou-Zeid et al. was 10 mm, although, for the purpose of modeling, the mortar was condensed into contact interfaces and removed from the geometry (See Section 3.7). At the top and bottom of the wall, 76 mm-thick steel clamps were used to help restrict the wall's movement during the blast's positive and negative phases. The exact dimensions of these steel clamps were not followed in the analysis because they were purely to create the structures boundary conditions set by the experimental setup. The experiment also used two sacrificial walls beside the CMU wall to help restrict in-plane movement and provide proper in-field blast wave interaction (Figure 3-1). This sacrificial wall was not modeled in Ansys and instead input as a variable in the model's boundary conditions.

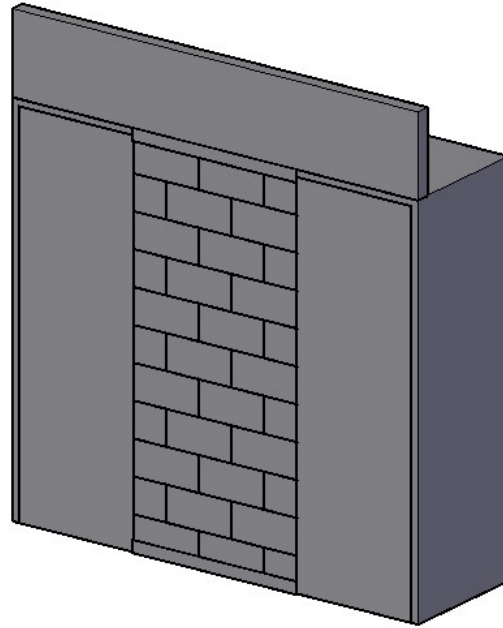


Figure 3-1: Abou-Zeid et al. Experimental Setup Rendition

Table 3-2: CMU Wall Dimension Summary

Object	Dimensions (Depth x Height x Length)
Standard Two-cell CMU	200mm x 200mm x 400mm
Single Cell CMU	200mm x 200mm x 200mm
Complete CMU Wall	200mm x 2200mm x 1000mm

3.4 PARTS

The only modeled portions of the wall are the concrete blocks and steel clamps, resulting in a total of three different modeled parts within Ansys Workbench. Shown below is the standard two-cell CMU (Figure 3-2-a), single-cell CMU (Figure 3-2-b), and steel clamp (Figure 3-3). The dimensions of these CMU parts are as shown in Table 3-2, with the steel clamp being an L-shaped bracket extending 76.2 millimeters along the backside of the masonry units. The final combination of all three parts representing a simplified version of the CMU wall experimental setup is shown in Figure 3-4.

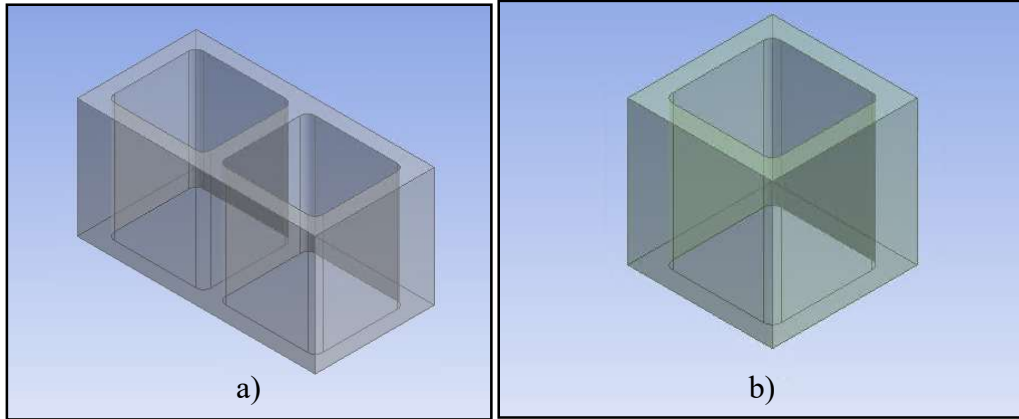


Figure 3-2: a) Standard Two-cell CMU, b) Single-cell CMU

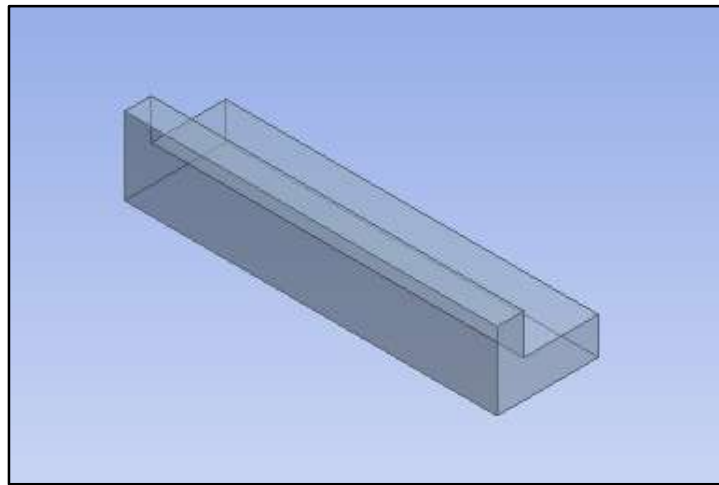


Figure 3-3: Steel Clamp

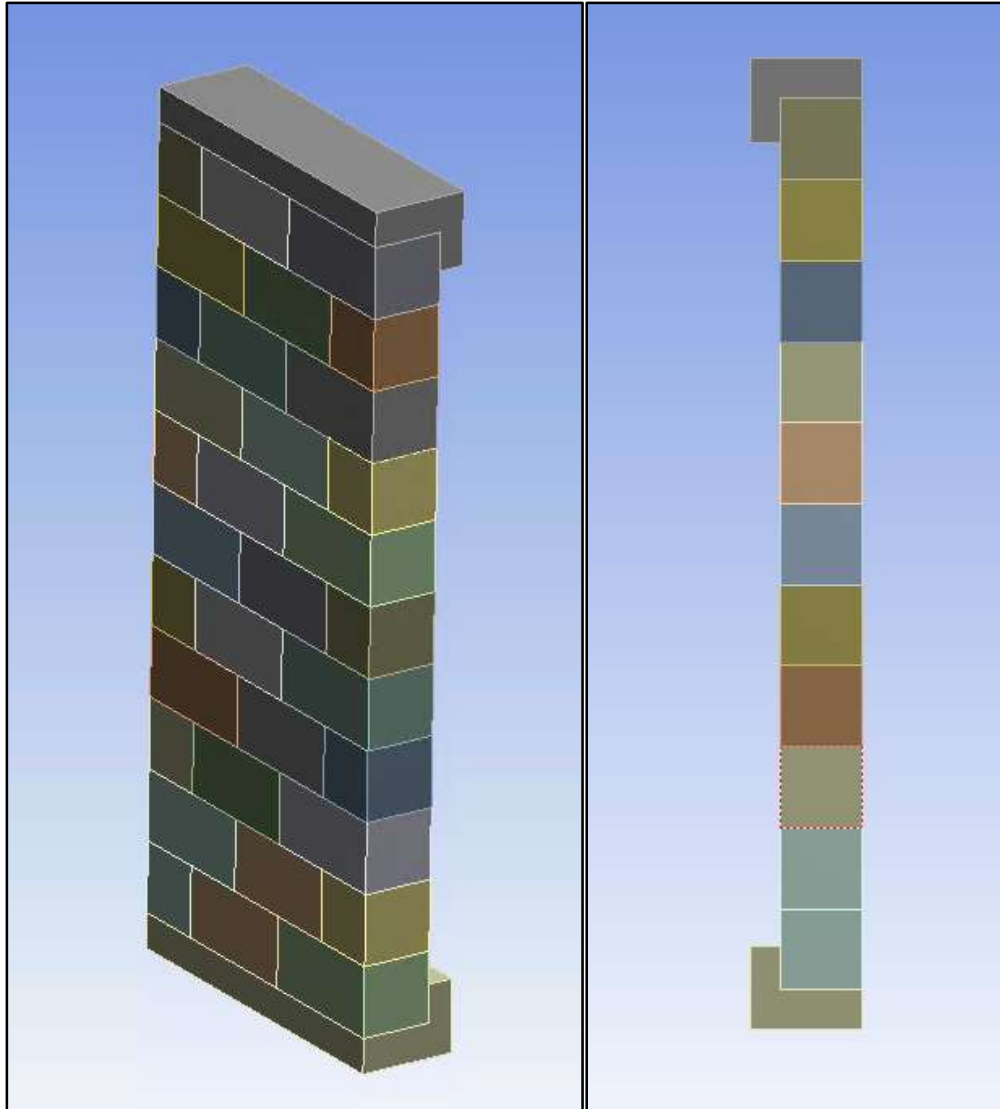


Figure 3-4: Isometric View (left) and Side View (right)

3.5 NODES AND ELEMENTS

Ansys Workbench has a mesh software that allows the mesh size to be automatically calculated or to be user defined. The mesh size plays an important role in the model during the analysis phase because it creates the sizes of elements and determines the number of nodes needed. The combination of the nodes and elements helps create the interaction between all the parts of the model and show the model interaction during the analysis phase. The Ansys Workbench auto-mesh feature was used for the original analysis and validation of the model using Lagrangian elements. This feature automatically determines a mesh size that makes equal amounts of elements within each part. Therefore, in Figure 3-5 the steel clamps have a much greater

element size than the single cell CMU. Since the steel clamp is not needed for the analysis, it is acceptable that its mesh size was not as refined. Using this auto-mesh feature resulted in a final node and element count of 138,304 and 89,343, respectively. The greatest size of each individual element was no greater than approximately 16 mm.

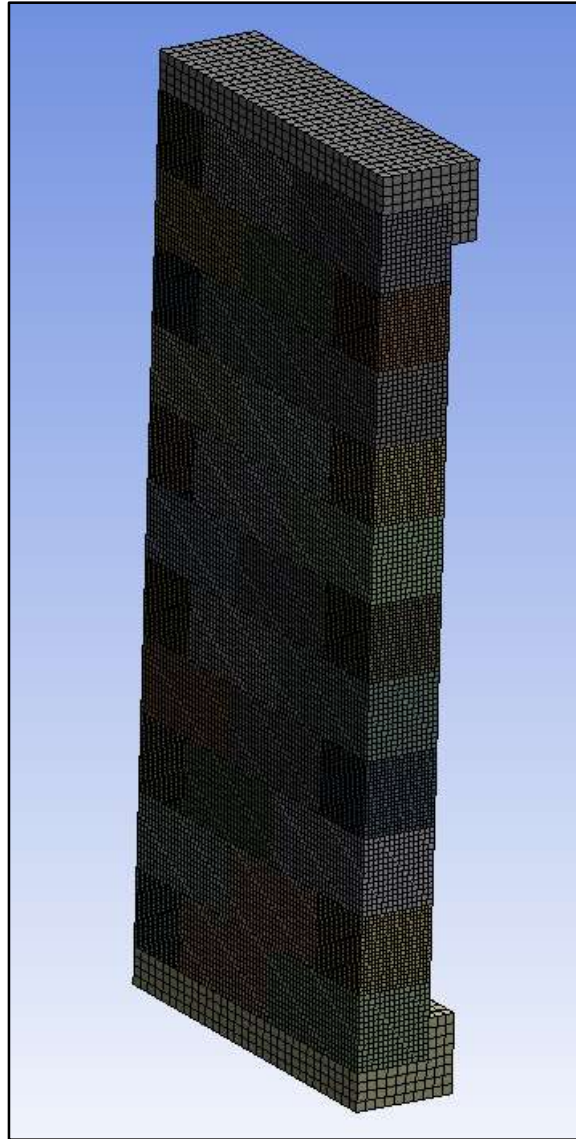


Figure 3-5: Isometric View with Wall Meshing

3.6 MATERIAL MODELS

Both Ansys Workbench and Autodyn have a wide range of material models that can be used in analysis. The most common materials are pre-defined with their corresponding material properties included in Ansys' database. These material models define how the material will

behave during the analytical phase. Even though these model types are pre-defined, the user can modify the specific material properties and even change the model type if need be.

For the analysis, only the properties of the concrete masonry units were needed, and they were modified to the standards set by Abou-Zeid et al.'s experiment. The behavior of the concrete used the pre-defined linear-elastic model and used the modified material parameters shown in Table 3-3.

Table 3-3: Concrete Masonry Model Parameters [30]

Parameter	Value	Unit
Modulus of Elasticity	200000	MPa
Poisson's Ratio	0.3	-
Compression Strength	13.79	MPa
Tensile Strength	0.52	MPa
Shear Strength	0.93	MPa
Density	2300	kg/m ³

3.7 CONTACT INTERFACES

After creating the model's geometry and applying material properties, it is important to define the surface interactions between each individual part in the system using contact interfaces. This definition of boundaries and interaction helps the model understand how all the parts interact during experimental conditions. For the wall used in the field experimentation, as well as any typical masonry wall, the masonry units are bonded together using a cementitious material. The wall used in this experiment had Type S mortar, which is typical for masonry construction, [16]. Due to the small size of the mortar joints (10 mm), it is common to not model the individual mortar layers between the masonry joints. Since the mortar acts as a bonding agent between the masonry units to create structural support, the user can model the mortar as a contact interface between adjacent masonry faces. Therefore, the mortar joints were condensed into contact interfaces. This contact interface then followed specific user-

defined stress criteria, which are stress limit states for the specific contact surface. For this model, wherever a masonry unit sat next to another masonry unit, the contact interface was defined to bond the two units together using the material properties of the mortar. If this stress criteria defined by the mortar properties was reached, the bond between the units would be broken. The mortar strength properties in Table 3-4 show the limits used to define the contact interface stress condition.

Table 3-4: Type-S Mortar Properties

Parameter	Value	Unit
Tensile Strength	0.45	MPa
Shear Strength	0.63	MPa

The CMU wall was placed in between steel clamps that simply held the blocks in position without any bonding or cementitious materials. To achieve this same interaction in Ansys, the CMU to steel clamp contact interface stress conditions were removed. This allowed these parts to interact separately which is identical to the experimental setup.

3.8 BOUNDARY CONDITIONS

Boundary conditions are sets of information that help to define the initial conditions and bounds for a given situation. For this model, it defines the imaginary point in space that the structure is confined to. These boundary conditions are then used to help solve for the remaining unknown deflection and pressure distribution values of the analytical solution. Depending on the problem being analyzed, there is a wide range of the possible amount of defined boundary conditions. For this model, only two boundary conditions were applied: a completely fixed and partially fixed condition.

The fixed condition was defined by the experimental model's steel clamps at the top and bottom of the wall segment. In the experiment, these clamps were made of solid steel and welded to a solid steel framed shipping container [30]. This prevented the masonry units from sliding out of plane during the blast's positive and negative phases. To replicate the steel

clamps condition within Autodyn, a 3-D fixed condition was applied to both steel clamps which completely restricted movement in all three axes (Figure 3-6).

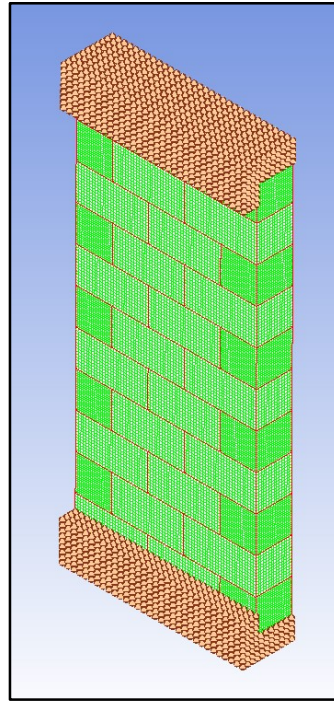


Figure 3-6: Steel Clamps with Applied Boundary Conditions

The partially fixed condition was defined by the experimental model's sacrificial sidewalls located on each edge of the wall segment. These sidewalls prevented the CMU from moving perpendicular to the blast loading and kept it bending in longitudinally. They also ensured that the blast wave would not reflect to the back face of the wall from wave reflections going inside the steel container. To replicate these sidewalls, an interactive boundary was placed along each edge of the model that restricted movement only in the axis perpendicular to the blast (Figure 3-7).

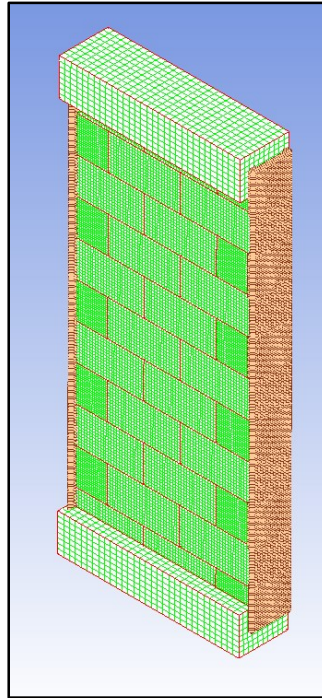


Figure 3-7: CMU Wall with Applied Boundary Conditions

3.9 LOADING

In the field experiment, the wall was not built with the intention to support gravity loads other than its own self weight [30]. Therefore, the only loading applied to the structure was the lateral blast load from the various charge weights, which were placed at ground level at their perspective standoff distances (See Section 3.11). Each charge in the experimental data used ANFO as the primary charge but required to be in terms of TNT for modeling. The ANFO charges were transformed into their equivalent TNT masses at a ratio of 1-kg ANFO to 0.87-kg TNT for modeling [12]. For the blasts at distances greater than 15 meters, they were also converted to scaled distances and scaled charge weights using ASCE 59-11 scaling laws.

3.10 BLAST MODELING

After the completion of the CMU wall in Ansys Workbench, the modeling of the blast wave was performed in unison with Ansys Autodyn for its primary focus on blast analysis. Two separate parts were formed to create the blast wave model: the atmosphere and TNT charge. For both the atmosphere and TNT, the model assumed that they would respond as an ideal gas.

The atmosphere was set as a 2-D Euler wedge element that extended the entire standoff distance of the given experiment (Figure 3-8).

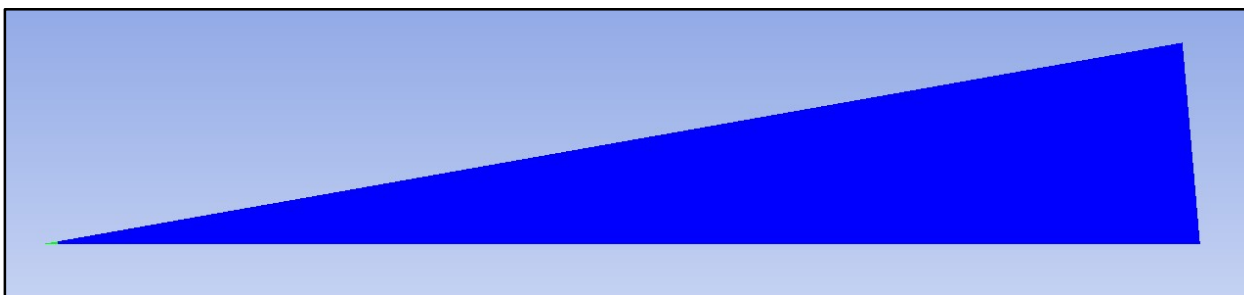


Figure 3-8: 2-D Wedge Atmosphere Element

The built-in properties of air as an ideal gas were then assigned to the wedge which was meshed with 10-mm long elements to create a completed “atmosphere” (Table 3-5).

Table 3-5: Air Model [31]

Parameter	Value	Units
EOS	Ideal Gas	-
Reference Energy	2.068×10^5	$\mu\text{J}/\text{mg}$
Reference Density	1.225×10^{-3}	g/cm^3
Air Pressure	101.3	kPa

Before inserting the TNT into the model, a single boundary condition was defined for the 2-D wedge atmosphere. The boundary condition labeled as “flow_out” within the Autodyn interface was used on the hypotenuse and vertical edge of the element (Figure 3-9). This “flow_out” definition allows flow to exit from the edges of the model space. Where this boundary condition was not defined, the software recognized this as an impenetrable barrier, or in the experimental case, the ground surface.

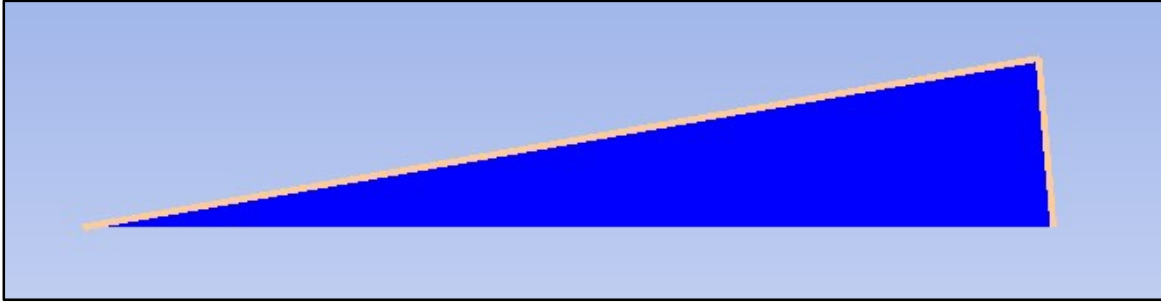


Figure 3-9: 2-D Wedge Element with Displayed Boundary Conditions

Next, the TNT charge was modeled in the system by creating a sphere at the corner of the wedge element and assigning it the properties of TNT (Table 3-6).

Table 3-6: Trinitrotoluene (TNT) Model [31]

Parameter	Value	Units
EOS	Jones-Wilkins-Lee (JWL)	-
A	3.738×10^8	kPa
B	3.747×10^6	kPa
R ₁	4.15	-
R ₂	0.90	-
W	0.35	-

To properly represent the TNT charge in model space, the Autodyn Manual specifies the following series of equations [31]. (Equation II provides the value to give the spherical charge a radius using the charge weight (w) in kg and the unit weight of TNT (γ) in kg/m^3 . While (Equation III and (Equation IV created the lower and upper bounds using the calculated radius and known standoff distance.

$$R = \sqrt[3]{\frac{3w}{4\pi\gamma}} \quad (\text{Equation II})$$

$$R_{min} = 10\% * R \quad (\text{Equation III})$$

$$R_{max} = \text{Standoff Distance of Charge} \quad (\text{Equation IV})$$

After finalizing the model, a detonation point was assigned to the center of the TNT charge (0,0,0) and allowed to initialize detonation at time zero. The blast was then allowed to run through the atmosphere until milliseconds before reaching the edge of the model (Figure 3-10). This pre-detonation of the charge allowed for a quicker and simpler modeling of the TNT blast wave before being imported into a complete 3-D model that combines with the wall. The various colors created throughout the middle of the wedge represents the velocity and direction of the force vectors. The red diamond at the beginning of the wedge shows the point of detonation for the TNT charge.

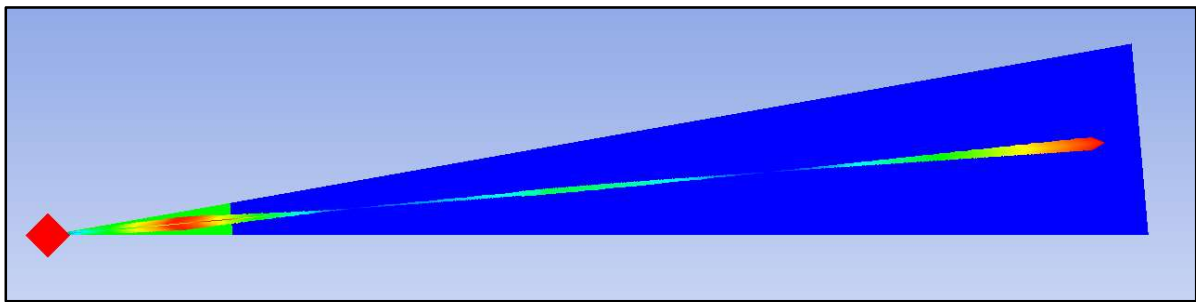


Figure 3-10: 2-D Wedge Element Containing TNT Charge and Atmosphere

This Autodyn model of the blast wave was then imported into the Workbench model. The combination of the two models converted the blast model from a 2-D wedge to a 3-D spherical element to coincide with the CMU wall parts in a single combined model (Figure 3-11). Within this combined model, gages were placed along the backside of the wall to record the displacement data during the analysis. The test was then run again, and time was given for the blast to properly interact with the CMU wall.

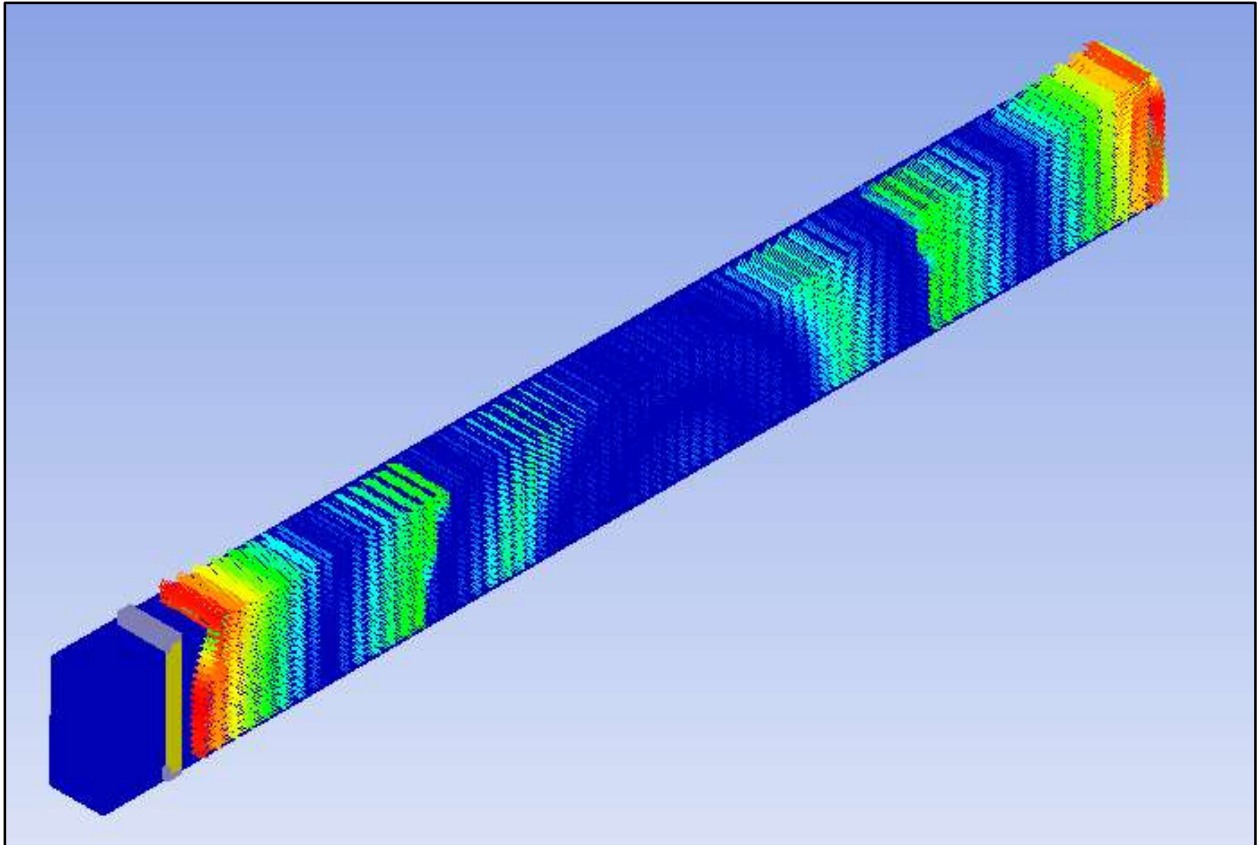


Figure 3-11: Complete Combined Model

3.11 MODEL VALIDATION

Before a model can be used as a representative simulation of a problem or an event, it must be validated using known data or proven formulations. Most often this validation process is completed simply by imitating real-world experimental data and comparing it to the results of the finite element model.

Depending on situational complexity, the process of completing a finalized and properly running model can take weeks, months, or even a year to complete. This is a result of the many factors that go into an experiment which can often include factors that go virtually unnoticed (e.g., current air pressures and frictional surface interaction). To make a model that represents verified data, all these factors must be accounted for and then properly inserted into computational software. Because of the many factors that can vary in a situation, these errors, or variations from the data are allowed while still confirming that a model is verified. This

allowance of error is not a single predetermined value that must be followed for all model validations. Instead, this value is determined situationally.

A combination of Abou-Zeid et al.'s experimental data and Kingery-Bulmash blast calculations was used to help validate the model results. Abou-Zeid et al. provided experimental data with various ANFO charges at given standoff distances with the resultant peak deflection (this is not equivalent to final deflection) and maximum reflective pressure. The Kingery-Bulmash blast calculations were used to ensure that the experimental blasts resulted in realistic reflective pressure values [32]. Once these pressures were confirmed, they were then cross referenced with the Autodyn blast simulation's peak incident pressure to ensure similarity.

Realistically, every experiment is expected to have imperfections no matter how precisely it is created. For the real CMU wall experiment, these imperfections and variation in properties can be in details such as: mortar strength, mortar to CMU bond, CMU weight and density, and explosive charge. It may also have small calibration errors in the deflection and blast pressure measurement devices along with human errors in during construction. On the contrary, a finite element model produces values that are known to be uniform and consistent at all levels. This difference in the level of imperfections means that a finite element model and true experimental model are expected and anticipated to not exactly match. With that said, the original goal for the model was to have the deflection values within a range of roughly 30%. As seen in the results summary (Table 3-7), this range was not met for all three loading scenarios.

Table 3-7: Model Results Summary and Comparison [30]

ANFO Charge (kg)	Standoff Distance (m)	Equivalent TNT Mass (kg)	Scaled Distance (m)	Model Peak Deflection (mm)	Experimental Peak Deflection (mm)
30	20	10	10	3.2	7
100	20	4	10	8.9	17
100	15	-	-	68.1	69

After further investigation into each of the scenarios' deflection-time histories, it was confirmed that even though their peak values differed, it still showed the model was reacting correctly to the blast wave. Shown in Figure 3-12 is the deflection-time history for the 100-kg ANFO charge at 15 meters produced within Autodyn.

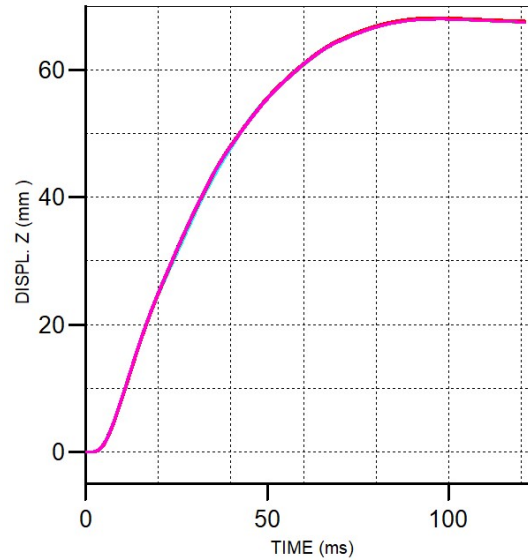


Figure 3-12: Ansys Autodyn Data (100 kg at 15 m)

At the peak displacement, the wall displaced as shown in Figure 3-13. At this point the individual wall components have moved separately from each other, signifying that the mortar joint have failed. This description of mortar joint failure being the only failed and visibly damaged component matches with the description of Abou-Zeid et al.'s experimental wall's performance.

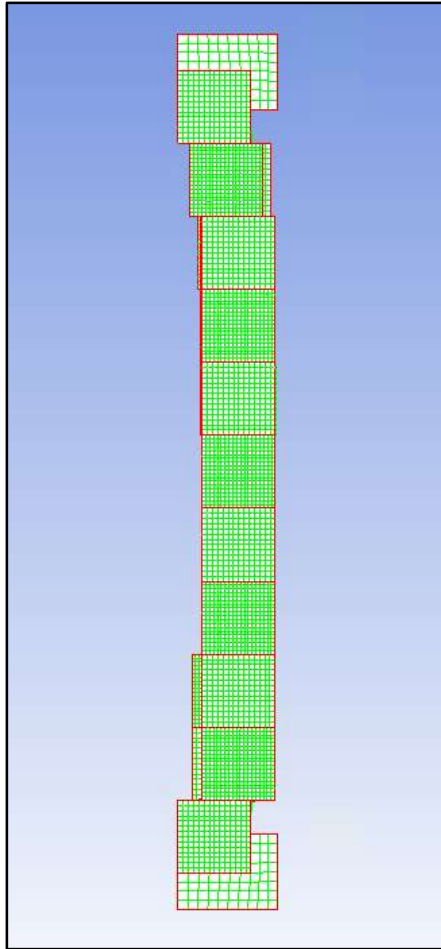


Figure 3-13: CMU Wall Model Post Blast

The scenarios producing the small deflections also have the greatest relative error. Although this percentage may be high, it is important to realize that the total difference between the model peak and experimental peak is relatively small. This greater difference in values may result from imperfections in the actual model as described previously. The investigation of both deflection-histories also reflects the shape and behavior seen in Abou-Zeid et al.'s graphical data. Both displacement-time histories for the 4-kg charge (Figure 3-14) and the 10-kg charge (Figure 3-15) are shown below.

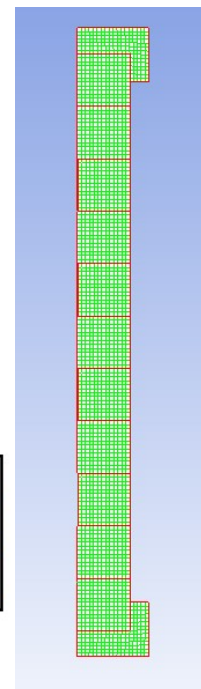
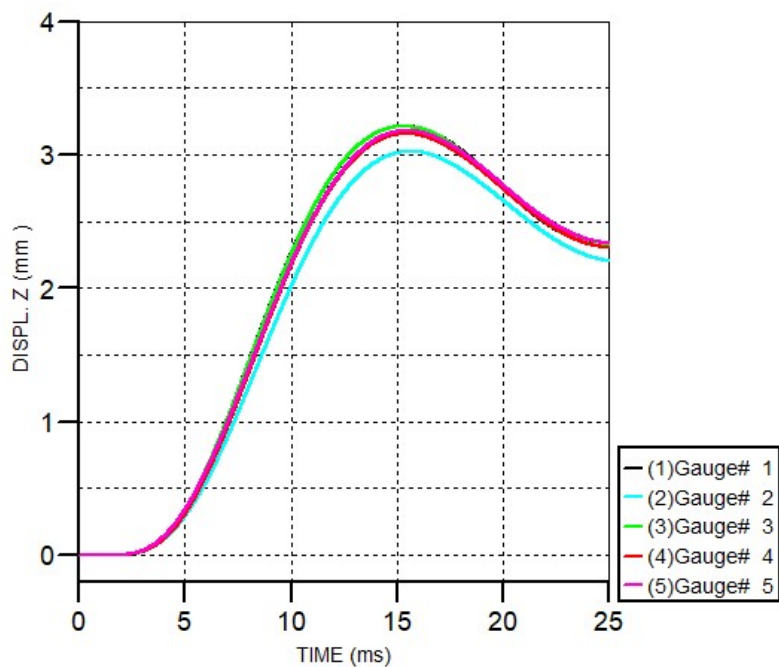


Figure 3-14: 4-kg ANFO Charge at 10 Meters

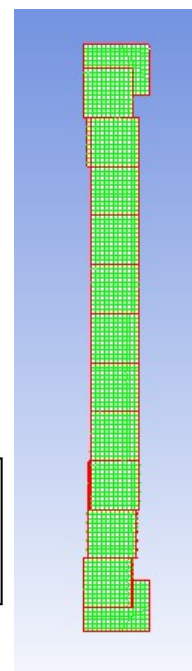
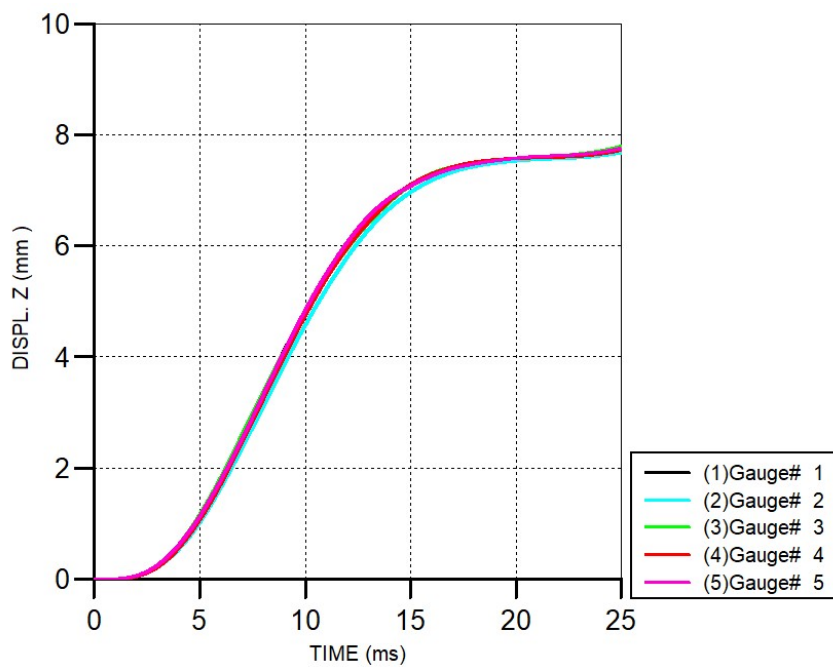


Figure 3-15: 10-kg ANFO Charge at 10 Meters

3.12 MESH SENSITIVITY ANALYSIS

In general, the mesh size will determine the accuracy of a finite element model. Using a fine mesh size to complete an analysis will provide more accurate predictions. Using a fine mesh size is not always the best option because it can impede on a computer's ability to process data in a reasonable amount of time. A mesh sensitivity analysis determines how changing the mesh size affects the accuracy of the results and the processing time and to find a balance between accuracy and the analysis time.

Initially, the mesh size was decreased to a much smaller uniform mesh size and the Autodyn analysis was rerun. After analysis was completed, the mesh size was increased in small increments and the analysis restarted. Each time the mesh was changed and analyzed; the results were compared. This continued until reaching a mesh size that saw considerable variation from the previous results.

When the mesh size approached approximately 25.4 mm, the deflection values increased by 10+ mm. It was also seen that a mesh this size was incorrectly distributing load across the wall. The wall had irregular areas of pressure in regions outside the joints, which is not accurate with the experimental behavior. The final mesh size selected was 19 mm for its similar results to the validated model and its relatively quick processing time of a maximum two days. For comparison, analysis of the original model took approximately five days. Figure 3-16 shows examples of the different mesh sizes and how they compare visually.

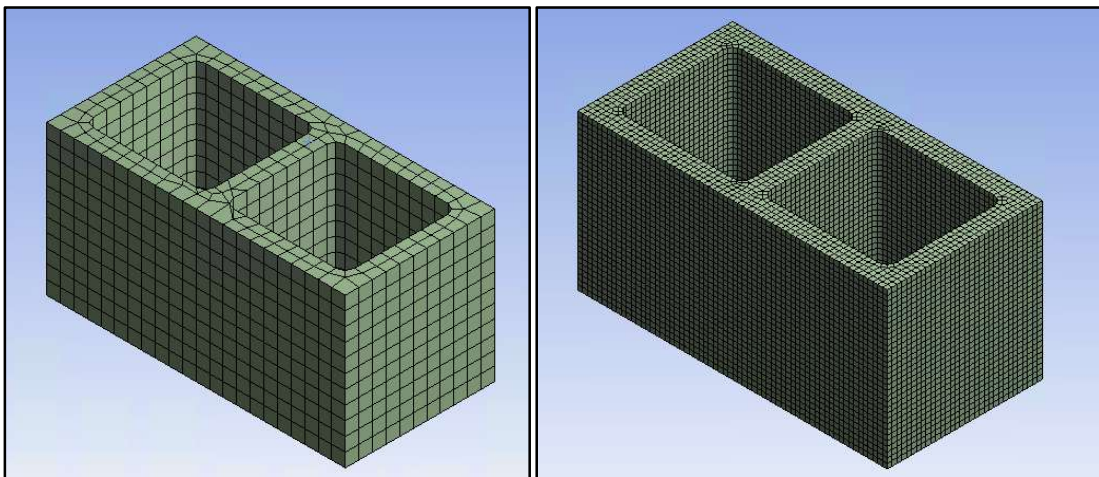


Figure 3-16: 19.05 mm Mesh (left) and 6.35-mm Mesh (right)

CHAPTER 4: PARAMETRIC STUDY

4.1 INTRODUCTION

As previously stated, unreinforced masonry walls are known to be weak when resisting lateral forces. In the event of an explosion, this means that unreinforced masonry walls are extremely vulnerable to destruction with high potential of harming those that the walls were built to protect. Unfortunately, in today's modern world, the occurrence of intentional blasting is becoming a more and more relevant topic around the globe. Because of this relatively recent threat, there has been little investigation into how to protect our existing structures against these scenarios outside of military applications.

There has been previous research that has investigated different methods to improve the strength of these walls with this vulnerability. This research includes, but is not limited to, the use of CFRP, GFRP, AFRP, polymer sprays, and polymer hybrids [7]. Out of this limited research, there is even less information being completed on using reinforced polymers for the strengthening of unreinforced masonry walls. Most research has focused on improving existing reinforced concrete beams, columns, and slabs using these materials.

The main objective of this retrofit analysis is to investigate how the addition of CFRP, Kevlar, aluminum, and mild steel to existing unreinforced CMU walls can improve wall strength against blast loading. Since we can expect structural components to fail under blasting, it is important to find ways of controlling how these components will fail. Ultimately, this is an investigation in how to protect the lives within these structures during a blast while preserving as much of the existing structure as possible. This blast load scenario does not apply to only acts of terrorism, but also applies to buildings containing the storage of any combustible material.

4.2 DIMENSIONS AND GEOMETRY

The dimensions and geometry of the modified CMU wall remained the same as in Chapter 3. The only difference is the addition of the composite materials, CFRP and Kevlar, to the backside of the wall face. These composite additions cover the full height and length (2200 mm x 1000 mm) of the wall while varying material thickness with each experimental run.

Since the composite materials act with the existing wall, the clamps were modified and extended to clamp both the material and CMU wall in place. For each change in the material thickness, a new modified model was created and analyzed separately.

4.3 PARTS

The CMU and steel parts used during the parametric study were the same parts used for the model validation. The only modification was the addition of new material added to the tensile face of the wall for retrofitting investigation. This new addition required creating a new part that took on the properties of the selected material. In this case, four new composite model sets were created using CFRP, Kevlar, aluminum, and steel.

Each part for the retrofit used the same dimensions and underwent the same Lagrangian meshing process. The mesh size remained 19 mm, resulting in 13,090 nodes and 6,372 elements for a 12.7 mm thick addition. After meshing was completed with the existing CMU wall (Figure 4-1), the wall was transferring into Autodyn to receive assigned material properties and material model sets.

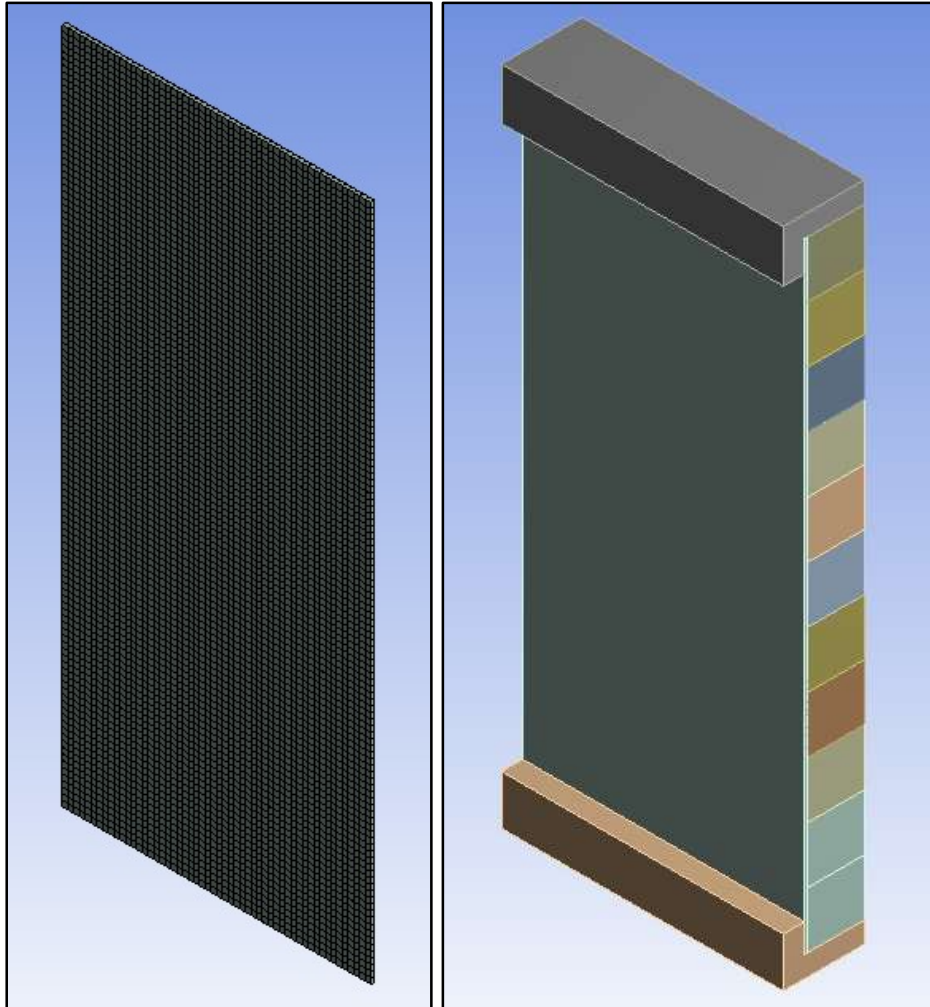


Figure 4-1: Meshed Retrofit Material (left) and New Composite CMU Wall (right)

4.4 MATERIAL SELECTION AND MATERIAL MODELS

The Autodyn software provides many different material properties and material behavior and failure models. Many materials have multiple selections that depend on the desired material behavior, failure model, element type, and strength. Therefore, many options are available when selecting a desired material. When selecting a material, it is important to note what element types were used in the model formulation. Since all the parts were created as solid elements rather than shell elements, only models applicable to solid elements were used.

The constructability of the retrofit was considered during the selection process for each material. The metals and fiber reinforced polymers were both bonded to the CMU in the same

manner using epoxy as the binding agent. This selection also ensured consistency in the model's parameters.

4.4.1 Carbon Fiber Reinforced Polymer

A high strength (395 MPa) pre-impregnated (prepreg) carbon fiber was selected for this analysis. The prepreg provided workability in applying the carbon fiber to the structure and consistent material properties. The pre-impregnated carbon fiber sheet allows for an even distribution of epoxy throughout the system that other application methods cannot achieve [24]. Therefore, the results from the finite element analysis provide more accuracy in the prediction of the actual application of CFRP to CMUs.

Table 4-1 provides the material model parameters defined within Autodyn.

Table 4-1: High Strength Prepreg CFRP Model Parameters

Parameter	Value	Units
Reference Density	1.54	g/cm ³
EOS	Ortho	-
Young's Modulus	9.45×10^6	kPa
Poisson's Ratio	0.4	-
Strength	Elastic	-
Shear Modulus	5.5×10^6	kPa
Failure	Material Strain	-
Tensile Failure	0.0031	-
Maximum Shear Strain	0.016	-

4.4.2 Kevlar

Autodyn provides two options for Kevlar application and modeling—an epoxied Kevlar and Kevlar fabric. When selecting either option it is important to consider how the material is being applied and utilized since the epoxy modifies the Kevlar properties and behavior. The Kevlar sheet morphs from being a loose and flexible fabric, to a much more rigid and firm

material. Since the application process uses epoxy to bind the Kevlar to the CMU surface, it was important that the epoxied Kevlar option was used.

Table 4-2 provides the material model parameters defined within Autodyn.

Table 4-2: Kevlar Model Parameters

Parameter	Value	Units
Reference Density	1.65	g/cm ³
EOS	Ortho	-
Strength	Elastic	-
Shear Modulus	5.5×10^6	kPa
Failure	Material Strain	-
Tensile Failure Strain	0.0031	-
Maximum Shear Strain	0.016	-

4.4.3 Aluminum

Aluminum is manufactured in many different alloys depending on its desired use. For this model, no specific aluminum was required; instead, the selection depended on the availability of aluminum model parameters within Autodyn. Therefore, aluminum alloy 7036 was selected. Unlike prepreg CFRP and Kevlar, the aluminum does not have any combination of aluminum and epoxy built into Autodyn. For aluminum, the epoxy is being used as the applicator to the CMU wall and the epoxy properties are used for the materials' contact interface. Table 4-3 shows the aluminum alloy 7036 model parameters used in analysis.

Table 4-3: Aluminum (AL 7036) Model Parameters

Parameter	Value	Units
Reference Density	2.77	g/cm ³
EOS	Shock	-
Strength	Johnson Cook	-
Shear Modulus	2.76×10^7	kPa
Yield Stress	3.37×10^5	kPa

Hardening Constant	3.43×10^5	kPa
Hardening Exponent	0.41	-
Strain Rate Constant	0.01	-
Strain Rate Correction	1 st Order	-

4.4.4 Mild Steel

Like aluminum, steel is produced in a wide range of alloys. For this analysis, the choice of using normal mild steel (4340 alloy) was used because of its high strength properties as well as it being a commonly used steel. 4340 alloy steel is a well-known alloy for its high levels of strength, toughness, corrosion resistance, and fatigue strength [33]. These properties have made it valuable in aircraft, automotive systems, tools, and machinery industries [33]. Therefore, the 4340 alloy steel should provide a desirable improvement in deflection values. The 4340 alloy model parameters are shown below in Table 4-4.

Table 4-4: Mild Steel (4340 Alloy) Model Parameters

Parameter	Value	Units
Reference Density	7.83	g/cm^3
EOS	Linear	-
Bulk Modulus	1.59×10^8	kPa
Reference Temperature	300	K
Specific Heat	477	J/kgK
Strength	Johnson Cook	-
Shear Modulus	7.7×10^7	kPa
Yield Stress	7.92×10^5	kPa
Hardening Constant	5.1×10^5	kPa
Hardening Exponent	0.26	-
Strain Rate Constant	0.014	-
Failure	Johnson Cook	-

4.5 CONTACT INTERFACES

When the composite materials were created inside Ansys Workbench, they automatically created contact interfaces to each CMU face and the surface of the composite material. This resulted in 33 individual interfaces for the same composite sheet, but with specifications bound to each individual masonry unit. Since the composite material is one continuous part needing only one bonding stress condition, all 33 automatically generated interfaces were replaced with a single grouped interface. This grouping simplified the model and reduced the potential error in manually typing 33 of the same bond stress conditions. Therefore, changing one set of values changed all 33 points of contact between the CMU and the composite material.

The bond stresses assigned to the contact interface limit states is shown in Table 4-5. These strength values came directly from the epoxy strength values listed by Master Bond within their product specifications [34].

Table 4-5: Bond Stress Values for Composite Material to CMU [34]

Parameter	Value	Units
Normal Stress	124.1	MPa
Shear Stress	27.58	MPa

4.6 BOUNDARY CONDITIONS

The only boundary condition applied to the retrofit material is the same boundary condition that is applied to the edges of the CMU wall. This boundary condition restricted the movement of the material in the direction perpendicular to the blast (Figure 4-2). It can be noted that this restriction assumes that the two side panels holding the wall in place remain. Since the retrofit material is simply an addition to the CMU wall, no other restrictions were required.

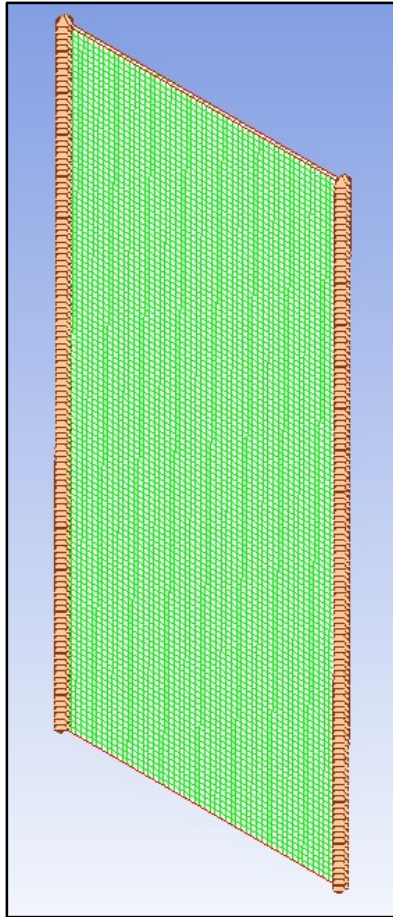


Figure 4-2: Material Addition with Defined Boundary Conditions

4.7 LOADING

For the parametric study, the wall was subjected to only one of the three blast loads used in the model validation. The blast scenario chosen was the 100-kg ANFO charge at a standoff distance of 15 meters since this charge was used as the representative choice for Abou-Zeid et al. figures and in a parametric study by Seyedrezai [35]. This loading scenario also showed the closest agreement with the finite element model when compared to the experimental results. The same calculated load model was applied to the load structure for each material added to the structure.

4.8 PARAMETRIC STUDY RESULTS

The objective for the data collection was to investigate the effects that each material had on the wall's peak deflection to establish which material provided the greatest overall protection

and stability. This investigation included factors such as material weight, material cost, constructability, and efficiency.

To ensure consistency in all tests, each model was run under that same blast loading conditions (100-kg ANFO at a 15-meter standoff distance and 159 kPa incident pressure) for the same material thicknesses and using the same bonding agent. The thickness for each material ranged from 3.175-mm to 19.05-mm in 3.175-mm increments. This provided six runs of each retrofit material (24 runs in total) of approximately 80-millisecond time frames. After completing each run, the results were compared to the control wall and its peak deflection of 68 millimeters.

4.8.1 CFRP Results

It is important to note that not all material thicknesses ran for the allotted 80 milliseconds for the CFRP. This was due to errors during the analysis file saving process which resulted in 60 millisecond time frames for the 3.175 mm and 15.875 mm tests. This also stopped the data collection for the 9.525 mm test at approximately 75 milliseconds. This inconsistency in end times was deemed acceptable as the desired peak deflection was recorded and the model was observed to behave properly before the termination of the analysis.

Post analysis, it was observed that the displacement-time histories showed a distinct peak displacement from the initial pressures followed by the structure decreasing in deflection during the negative pressure phase (Figure 4-3). The CFRP retrofit behavior followed the expected curvature provided by the control CMU wall data. The various material thicknesses resulted in wall displacements ranging from a maximum of 48 millimeters to a minimum of 22 millimeters.

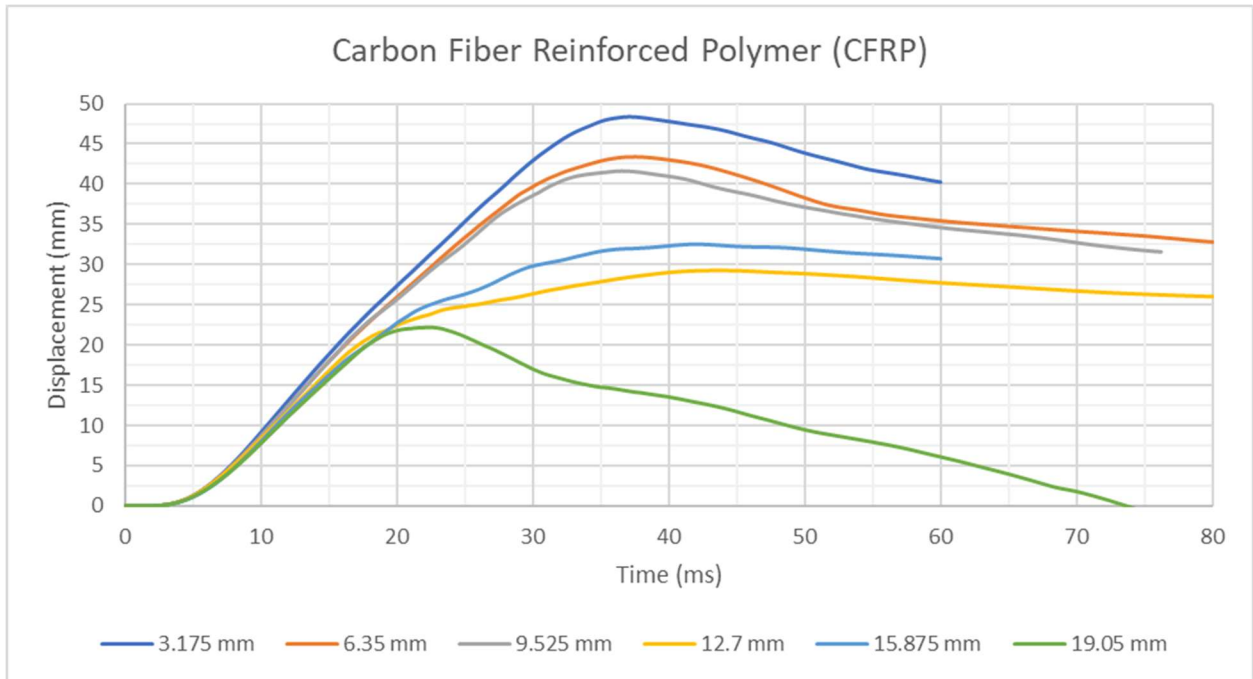


Figure 4-3: Ansys Autodyn Model Displacement-Time History Results for CFRP

Within each model containing a new material thickness, Autodyn recreated and recalculated the mesh sizes and interactions between each surface. Therefore, each model was expected to have variation in deflection data. This can be observed in the graphical data for CFRP thicknesses 12.7 mm and 15.875 mm. In theory, the 15.875-mm thick addition should produce values that are lower than that of the 12.7-mm thick addition, but it instead has a greater deflection value by approximately three millimeters. It was concluded that with the linear increase of material thickness there was a linearly decreasing result in peak deflection values.

Beyond looking at expected deflection-time histories, it was also important to investigate the model's behavior in failure. Post-blast damage in the control wall was primarily in the mortar bed joints [30]. Figure 4-4 provides a snapshot of the wall post-blast for the 3.175-mm thick CFRP at its approximate peak deflection and where the failures are occurring. Each observed failure point in the model is found along the mortar joints in the wall which allowed the wall to move and deflect under the lateral pressure. This same pattern was observed with the remaining CFRP thicknesses, with the amount of failure between each block decreasing with material thickness.

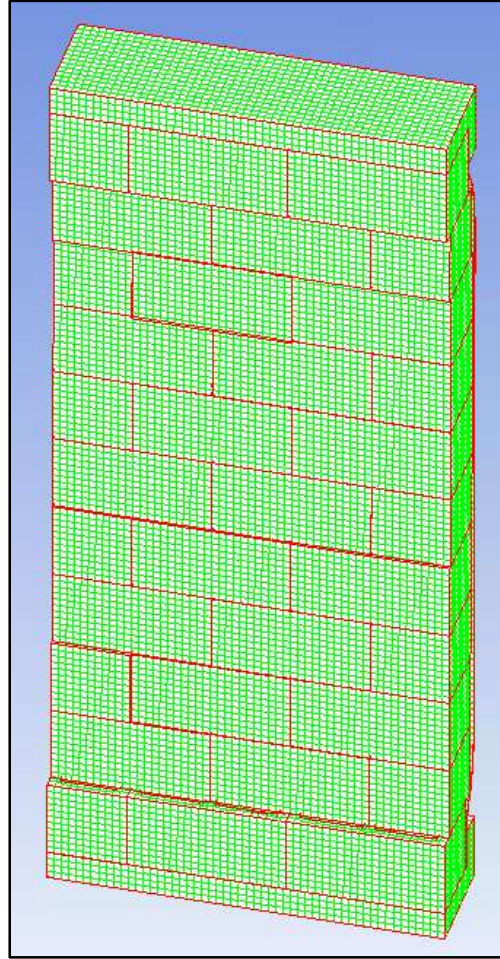


Figure 4-4: 3.175-mm Thick CFRP Retrofit During Peak Displacement

Figure 4-5 reflects the resultant peak deflection and its percent improvement from the original control wall's peak deflection. The percent improvement represents the peak displacement seen at the material thickness divided by the control displacement of 68 millimeters. This data is used as an aid to show how effectively the CFRP performed at each thickness.

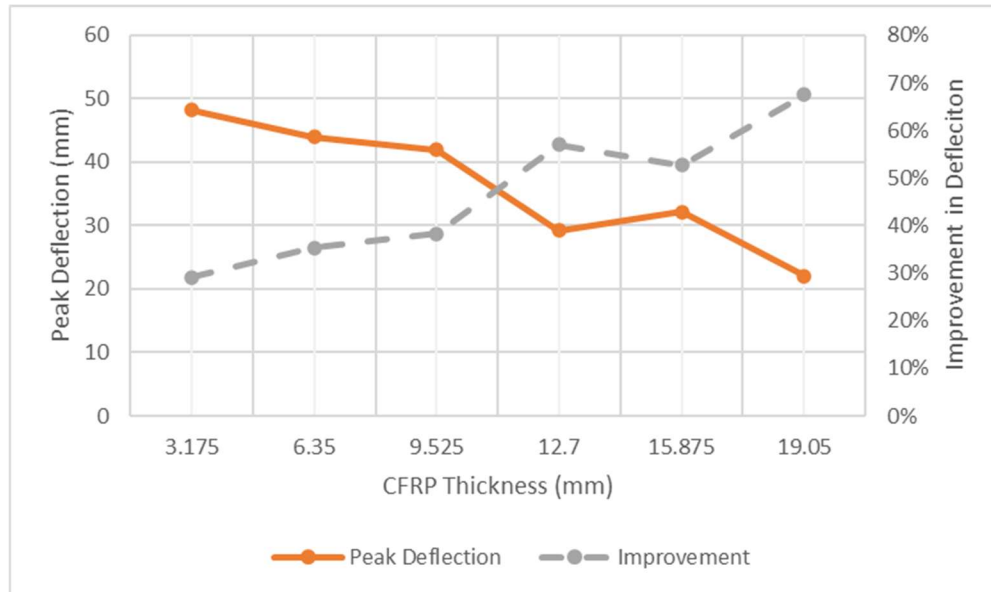


Figure 4-5: Peak Deflection and Percent Improvement in Deflection for CFRP

4.8.2 Kevlar Results

For the Kevlar model displacement-time histories, there is a clear displacement peak followed by a displacement rebound which again matches the behavior of the control wall (Figure 4-6). Each increased material thickness resulted in a decrease in the peak displacement values. The graphical data for each individual curve also consistently follows the same trend before and after the peak. The only run with more variation from the control is the 12.7-mm thick Kevlar. Even though that this run provides some variation from the trend, its peak lands in the expected region when compared to the other thickness curves. The highest deflections seen by the Kevlar reinforced wall across all thicknesses was approximately 45 millimeters with the lowest deflections reaching approximately 24 millimeters.

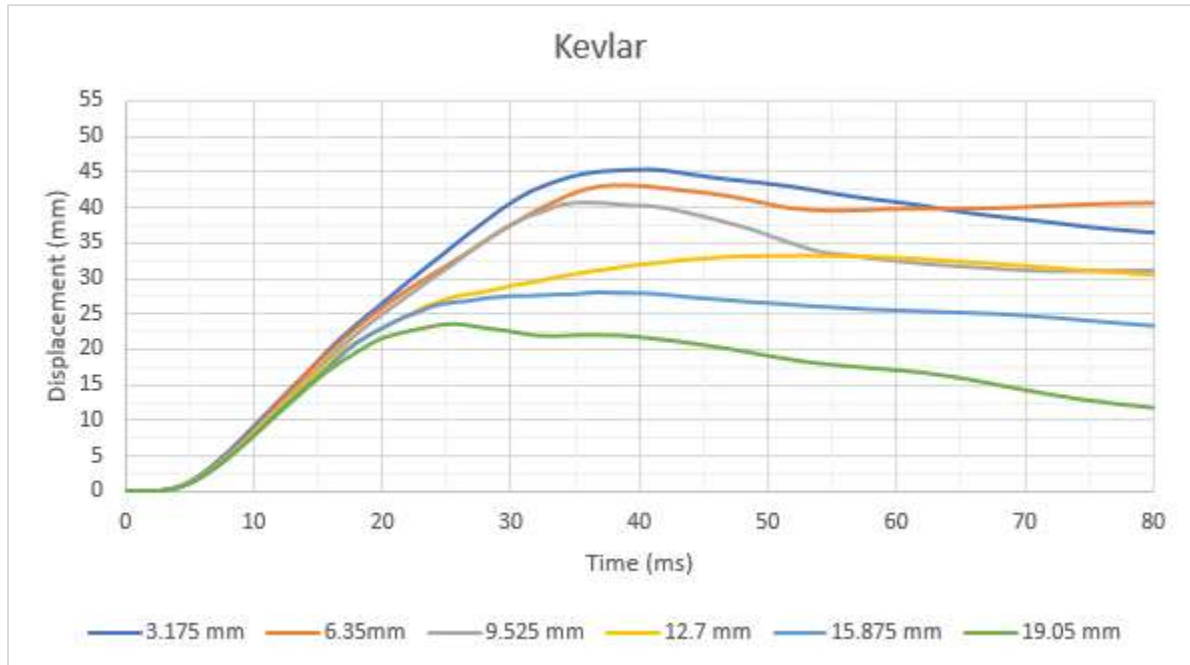


Figure 4-6: Ansys Autodyn Model Displacement-Time History Results for Kevlar

Like the CFRP-CMU wall behavior, the Kevlar addition showed the same modes of failure as seen in the control. All the failures occurred only at the mortar joints which was the main cause of the structure's deflection. Figure 4-7 shows the 3.175-mm thick Kevlar model at its peak displacement. This model resulted in the highest levels for displacement and showed the greatest movement between the joints.

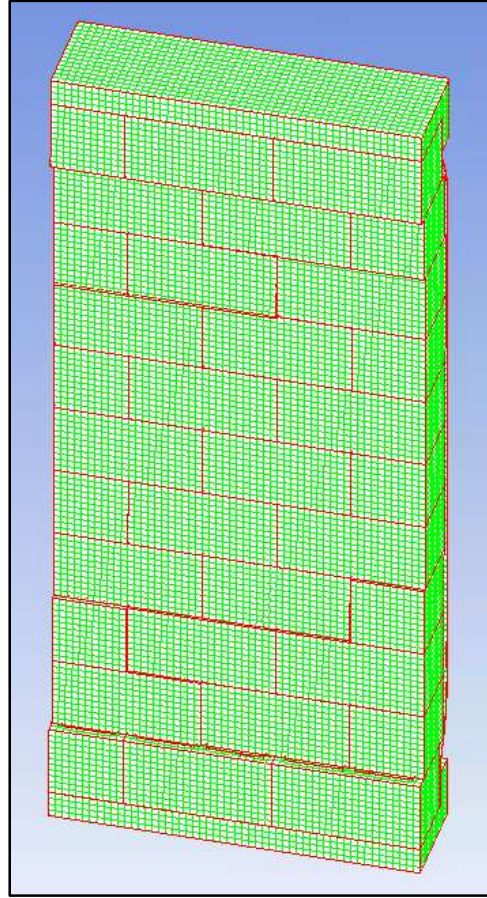


Figure 4-7: 3.175-mm Thick Kevlar Retrofit During Peak Displacement

Figure 4-8 reflects the resultant peak deflection and the Kevlar's percent improvement from the control wall's peak deflection of 68 millimeters. The Kevlar showed to linearly improve the CMU wall from 34% to nearly 65%.

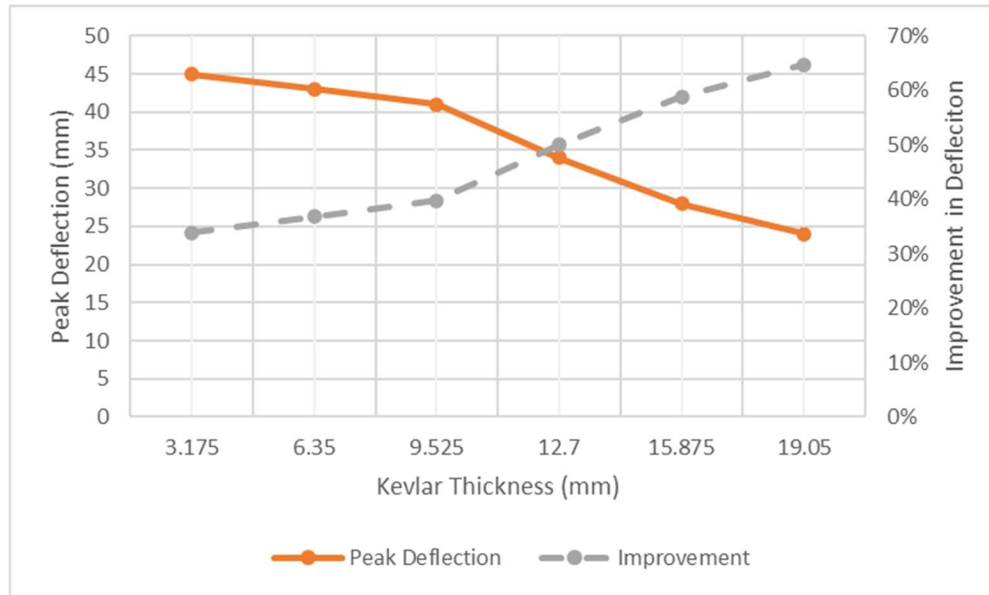


Figure 4-8: Peak Deflection and Percent Improvement in Deflection for Kevlar

4.8.3 Aluminum Results

The results for the aluminum time-history curves followed the displacement-time history from the control data. Although, when analyzing the entire time-history for the aluminum, there is a considerable amount of variation in the curve behavior of the material (Figure 4-9). Thicknesses ranging from 3.175 to 9.525 millimeters appear to follow similar curves, while thicknesses 12.7 to 19.05 millimeters follow a different curve. This variation could be a result of the aluminum model selected within Autodyn and how it chose to interpret the geometry. Even with this variation, the resulting peak displacements at each thickness still produce a predictable and linear pattern that decreases with the increase in material thickness.

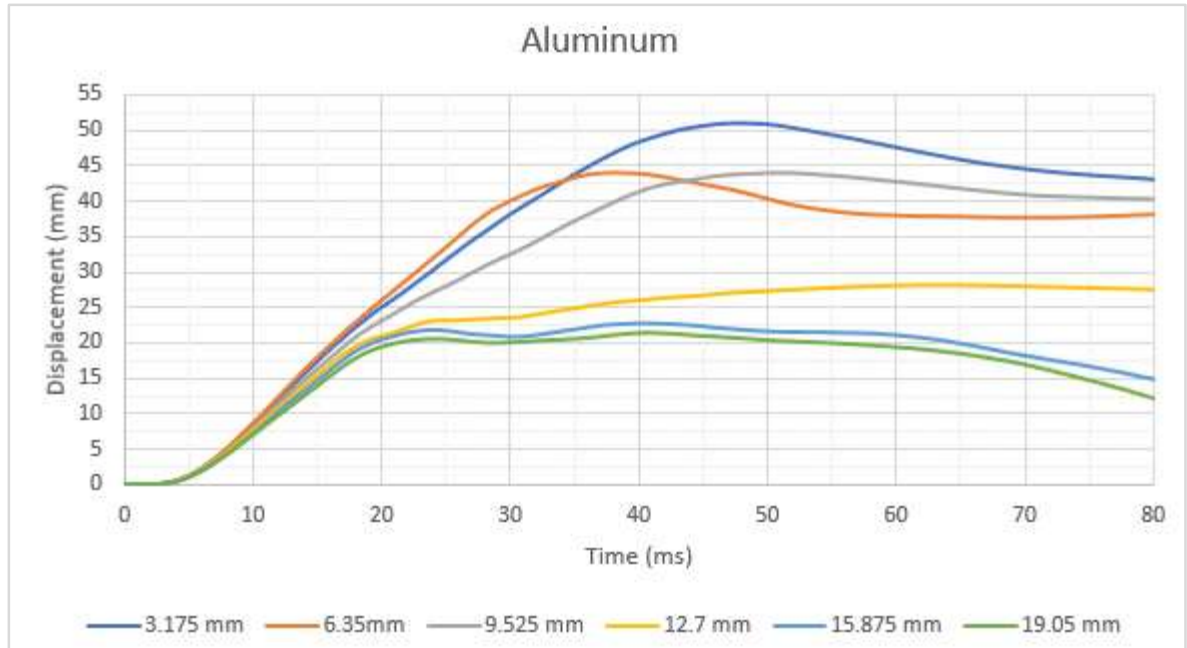


Figure 4-9: Ansys Autodyn Model Displacement-Time History Results for Aluminum

The CMU walls fail in the same manner with each aluminum thickness. Figure 4-10 shows the aluminum during its highest peak deflection during the 3.175-mm thick retrofit. Each model resulted in failure at the mortar joints with slight variations in specific mortar joint breakage for each run. These similarities validate that the model is behaving similarly in all runs.

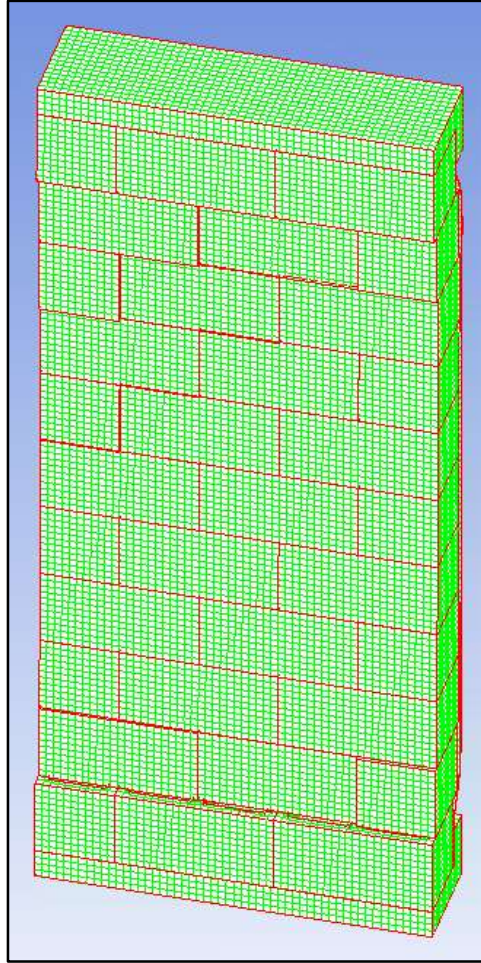


Figure 4-10: 3.175-mm Thick Aluminum Retrofit During Peak Displacement

The aluminum showed to have the greatest difference between the maximum peak displacement and the lowest peak displacement values when compared with the other retrofit materials. When comparing this data to the control CMU wall, the aluminum sees a range of 25% to 69% deflection improvement (Figure 4-11).

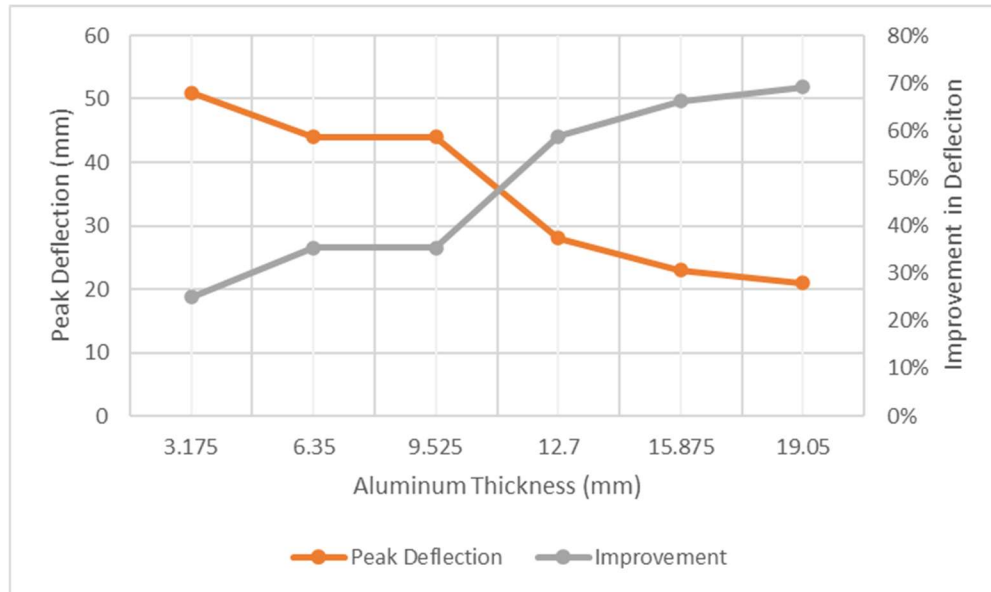


Figure 4-11: Peak Deflection and Percent Improvement in Deflection for Aluminum

4.8.4 Mild Steel Results

The displacement-time history for the mild steel showed great consistency in each curve's behavior, with the only exception being the 3.175-mm thick reinforcement (Figure 4-12). It is possible that this point, reaching a peak displacement of 43 millimeters, is an outlier from the data because of error within the finite element analysis. At each variation in thickness, it still follows the same displacement-time behavior as the other thicknesses and the control. Considering the possible outlier, the maximum and minimum peak displacements were approximately 43 and 14 millimeters, respectively.

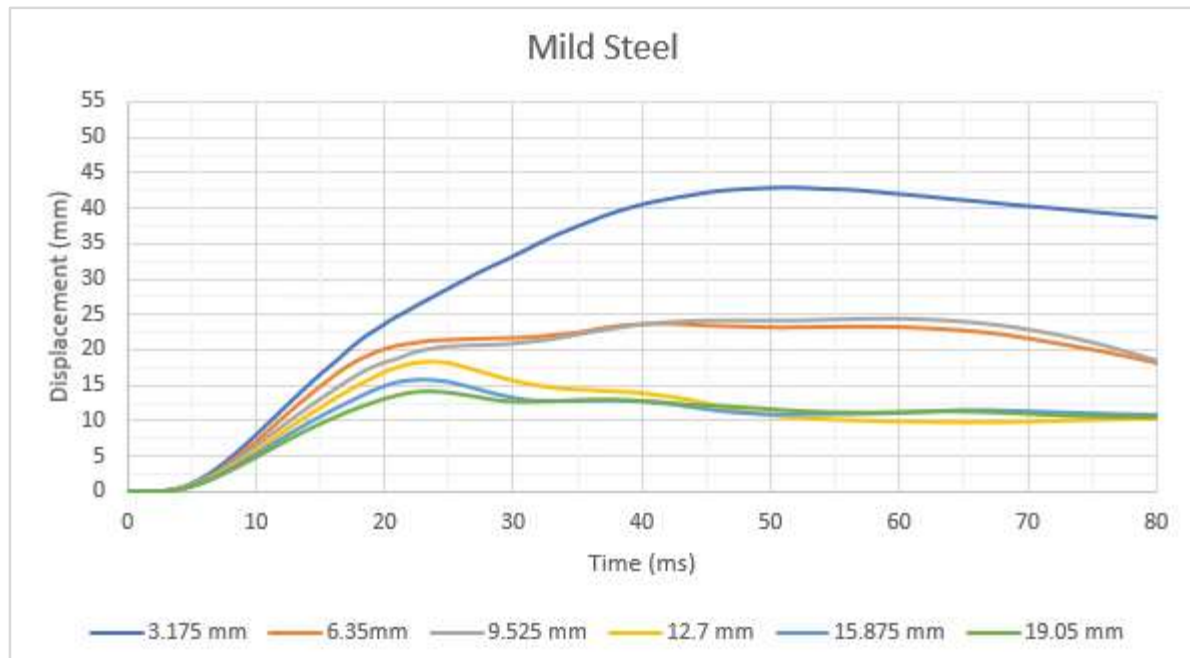


Figure 4-12: Ansys Autodyn Model Displacement-Time History Results for Mild Steel

When observing the peak displacements of each steel model, the steel plating resisted the most amount of deformation and provided more lateral resistance for the CMU wall. Figure 4-13 shows the peak displacement for steel for the 3.175-mm thick reinforcement and the locations of the failed joints. The steel showed the least number of failed joints in the system compared to the other reinforcement materials. Since this is the addition of steel to an unreinforced CMU wall, this scenario is analogous to a reinforced masonry wall, which has steel reinforcing bars implemented within the masonry cells. Reinforced masonry has much better resistance against lateral loading. Therefore, steel addition should in fact decrease the wall's deflection significantly. Figure 4-14 shows the wall's peak deflection and how the steel reinforcement provided 37% to 79% improvements in peak wall deflection.

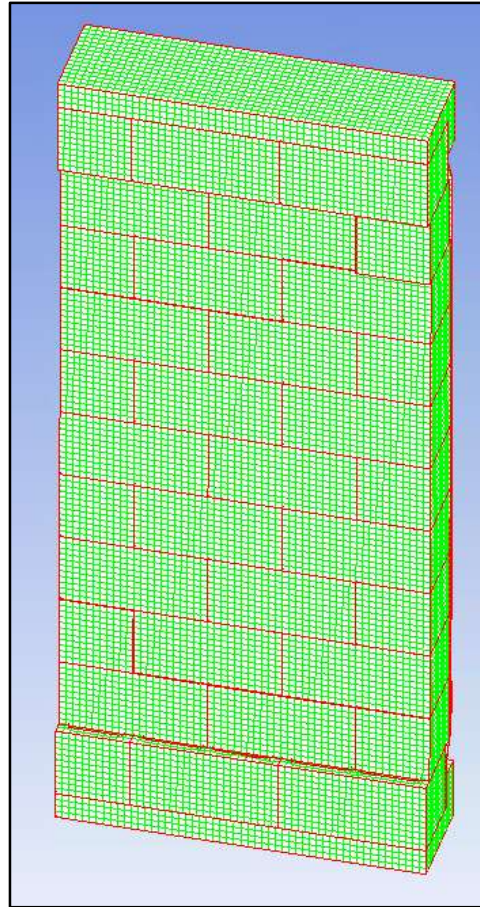


Figure 4-13: 3.175-mm Thick Steel Retrofit During Peak Displacement

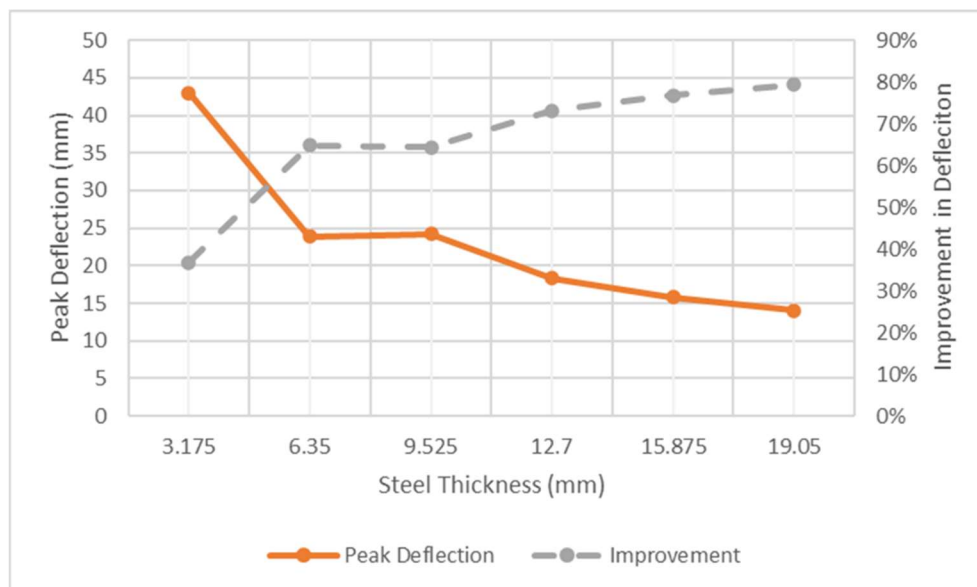


Figure 4-14: Peak Deflection and Percent Improvement in Deflection for Mild Steel

4.8.5 Combined Summary of Results

A complete summary was created to compare all materials behaviors and determine the best option for retrofitting unreinforced CMU walls against blast loading.

The results of the Kevlar model matched closely with the CFRP model. These results are not surprising, as they both are reinforced polymer materials that are known for their high strength to weight ratios [18, 25]. The main differences are that Kevlar is commonly used for its excellent resistance against penetration, while CFRP is superior against creep [19, 23]. Since their behavior against significant dynamic loading is a relatively new area of study, their similar results are reliable. In a test by Muszynski and Purcell [36], the main difference found between a Kevlar/glass hybrid and CFRP is that the Kevlar/glass hybrid resulted in a more ductile failure. This same observation can be seen in the finite element model results when comparing the curve behavior post-peak displacement for CFRP and Kevlar.

An important note for the use of both the aluminum and mild steel models is that they also have been applied using epoxy adhesive. This type of application could potentially affect the results of using other methods of application, such as anchoring or bolting, because these methods would affect the overall boundary conditions. The reason for the selected application for this retrofit investigation was to limit the amount of changed parameters between each material.

When comparing each material, CFRP, Kevlar, aluminum, and steel, the steel proved to have the smallest peak deflection values at each level of thickness using the control charge weight. Table 4-6 provides a summary of each material and its response at the given material thickness, while Figure 4-15 provides a visual representation of the recorded data and its behavior at each thickness.

Table 4-6: Peak Deflection Results for All Materials

Material Thickness (mm)	CFRP	Kevlar	Aluminum	Steel
3.175	48.2	45	51	43
6.35	44	43	44	23.9
9.525	42	41	44	24.2
12.7	29.2	34	28	18.3
15.875	32.2	28	23	15.8
19.05	22.1	24	21	14

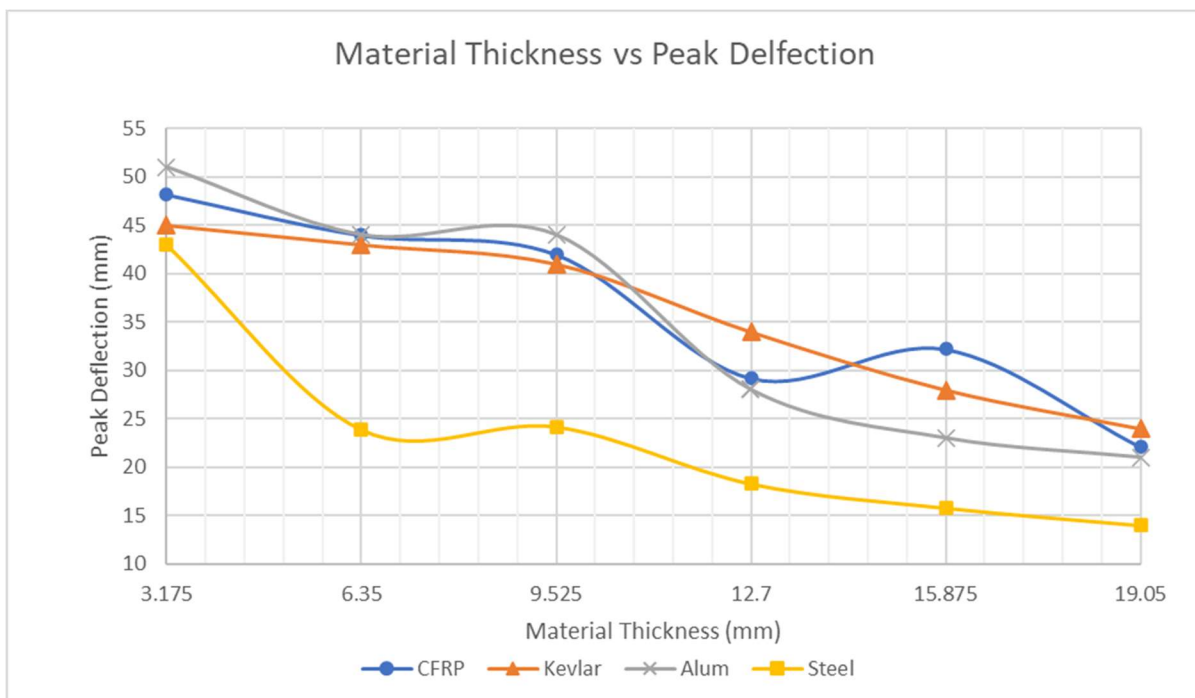


Figure 4-15: Peak Deflection Results for All Materials

The main purpose of this analysis was not merely to identify the peak displacements of the material, but to see how these peak displacements compared to the control wall deflection values of 68 mm. This is important because the lower the wall deflection, the decreased chances of wall failure and potential harm to life. In conjunction with the previous graph, the

steel easily provides the greatest percent improvement in deflection for each thickness. The tabulated and graphical representations of the results is shown in Table 4-7 and Figure 4-16, respectively.

Table 4-7: Improvement in Peak Deflection for All Materials

Material Thickness (mm)	CFRP	Kevlar	Aluminum	Steel
3.175	29%	34%	25%	37%
6.35	35%	37%	35%	65%
9.525	38%	40%	35%	64%
12.7	57%	40%	35%	64%
15.875	53%	59%	66%	77%
19.05	68%	65%	69%	79%

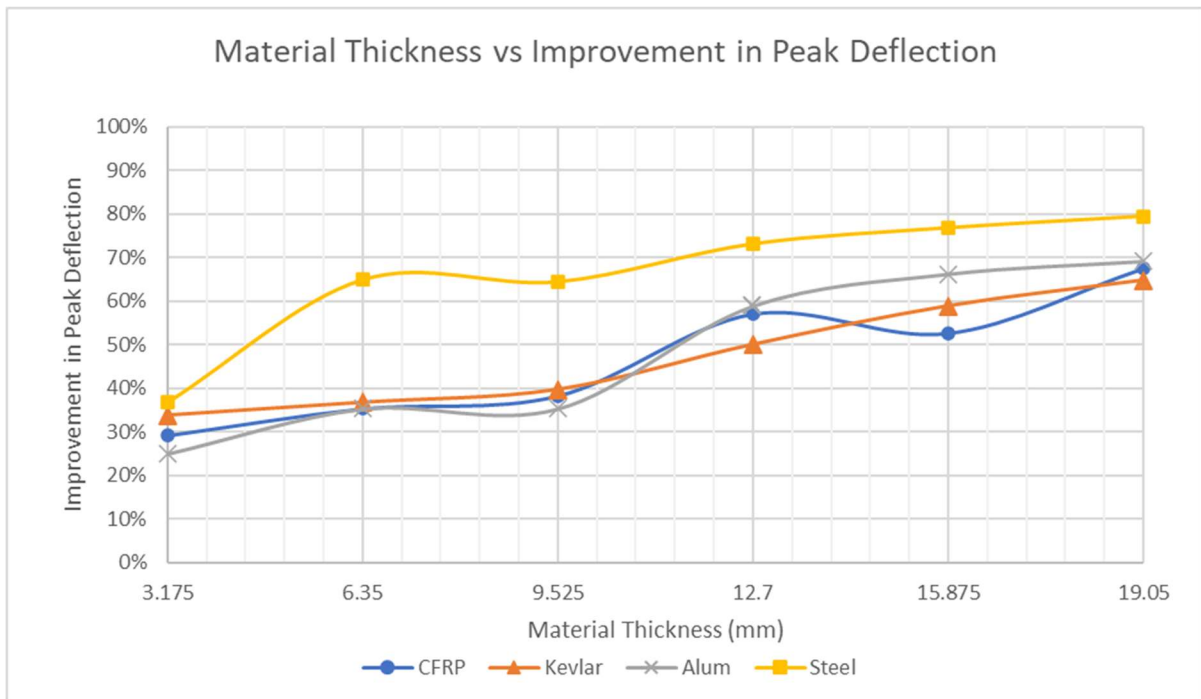


Figure 4-16: Improvement in Peak Deflection for All Materials

Design loads are fundamental in the design process and a controlling factor for member sizes and overall structural capabilities. Understandably, the more load that we have applied to a structural member the larger member size we will require. This in turn requires a greater amount material which typically results in higher costs. Therefore, the factor of weight for the material addition should be considered in deciding the best material retrofit option. Figure 4-17 displays how much weight is required of the material to achieve one percent of wall deflection improvement. Steel, while being the densest material, also proved to achieve the greatest improvement in peak deflection. This shows that even though it provided great results, it weighed significantly more. Both the CFRP and Kevlar materials showed that they provided the greatest improvement per unit weight added to the structure. In the previous graphs for deflection data, the aluminum followed the behavior and values of the CFRP and Kevlar materials relatively closely. Comparing the deflection to the weight per percent improvement in deflection, it shows that even though the aluminum performed similarly, it did so with a significantly higher weight.

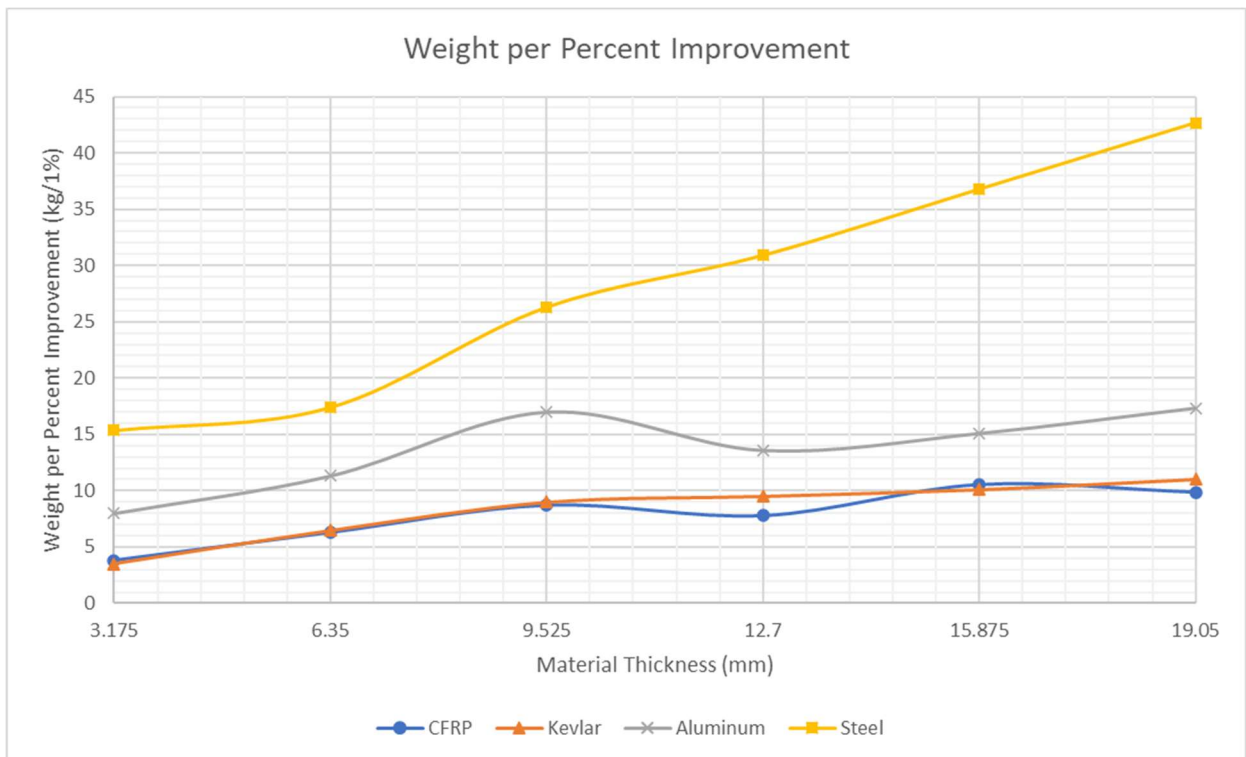


Figure 4-17: Weight per Percent Improvement in Deflection

Lastly, when choosing the method of retrofit, it is important to investigate the costs for each method. Since the funding for a project can control what resources are available to you, it can require the use of cheaper less efficient materials. At the current (2020) market values for raw material, plain weave fabric Kevlar is the most economical at \$0.69/kg and aluminum being the costliest at \$4.56/kg (Table 4-8). Although, it is important to look at the total amount of material weight that is needed for a project. Referring to Figure 4-17, it shows that even though steel is not the costliest material per unit weight, it does require far more material mass than the alternatives. Another important factor not included in Table 4-8 is that these values (with CFRP as an exception) do not include the price of the epoxy that would be used during the application process. One of the recommended laminating epoxies from Fibre Glast Developments Corporation costs approximately \$500 for an 18.9-liter pail (18.14 kg) [39]. Therefore, this price increase would need to be factored upon the material requirements of the retrofitting project.

Table 4-8: Material Cost for CFRP, Kevlar, Aluminum, and Steel (2020 Market Values)

Material Quantity	CFRP - Prepreg [37]	Plain Weave Fabric Kevlar [38]	Aluminum [40]	Carbon Steel [41]
Per kg	\$1.78	\$0.69	\$4.56	\$0.84

4.8.6 Comparison with Literature

The literature on blast loading for masonry structures shows many differences in the variables used during analysis. These variables can create difficulty in comparing running bond orientation, reinforced or unreinforced masonry, material strength, peak pressures, and even material thicknesses. Each factor is important for the wall's structural integrity and the response. Although, even with these factors we can still compare the observed behavior and experimental relationships.

For example, Ehsani et al. performed a blast loading test on a plain non-bearing unreinforced masonry wall with no mortar between or inside the cells and the same wall with CFRP reinforcement on both wall faces. Ehsani et al. observed that the completely unreinforced wall experienced total collapse, while the CFRP wall saw a peak displacement of 228.6 millimeters

and rebounding behavior [42]. This experimentation was done to create a “worst case scenario” type event and to see how the addition of CFRP would affect the situation. This experiment helped show how wall CFRP can perform under extreme loading conditions.

Muszynski and Purcell conducted blast testing on unreinforced air-entrained concrete (AEC) masonry walls and concrete walls both reinforced with 3-ply (1.5-mm thick) CFRP and Kevlar/glass hybrid materials [36]. The masonry wall was constructed within a reinforced concrete frame and had structural steel angles surrounding the wall edges and laminate materials. Post-blast observations showed the CFRP and Kevlar/glass hybrid decreased the concrete wall deflection by 25% and 31%, respectively. The masonry wall with CFRP and Kevlar/glass had decreased deflection from 10-31% and 30-44%, respectively.

Carney and Myers tested twelve unreinforced masonry walls retrofitted with strips of glass fiber reinforced polymers. When compared to the control walls, the retrofit showed an increase in wall strength by a factor of two, cutting the wall’s deflection in half [7]. Experimental testing performed by Myers et al. using GFRP resulted in a similar conclusion [7].

Crawford et al. performed a finite element analysis using DYNA3D and static experiments to examine the effects of using AFRP to retrofit a CMU wall [7]. Crawford et al. concluded that using AFRP decreased the wall’s deflection by approximately 60% when compared to the control wall.

Overall, the results from published works help to show that the results from this finite element model land within reasonable bounds. Due to variation in each experimental setup and formulation, it is expected to not match the exact results of all scenarios.

CHAPTER 5: CONCLUSIONS AND RECOMMENDATIONS

5.1 CONCLUSIONS FOR RETROFITTED UNREINFORCED CMU WALLS

When comparing all materials in terms of deflection, the mild steel retrofit application proved to be the best. Mild steel had the lowest peak deflection values (43 mm to 14 mm) and the highest total percent improvement in peak deflection (37% to 79%). Although the steel performed best in deflection reduction, the steel is not the most realistic option to use in retrofit design. Using steel would require the pre-fabrication of metal panels to conform to the geometry of the structure before installation. This pre-fabrication makes it difficult to work with on-site, especially since they are large solid steel sections that must work around an existing structure. If the structure is not straight, this also adds an extra level of difficulty during application because of the steel panel's workability. Using steel to retrofit a non-load bearing wall also will add a great amount of extra weight because of the steel's high density. This added weight also means extra cost to the stakeholder that is making retrofit alterations to the structure.

Aluminum, much like steel, proved to be efficient in decreasing the peak deflection of the CMU wall. Although, just like steel, the aluminum does not provide the best alternative in the form of workability. Using thick aluminum panels is not easily workable and would require the shaping of the metal before being applied to the structure's surface. Aluminum, being a third of the density of steel, would not create such an immense increase dead load to the CMU wall, but would come at almost four times the cost to apply.

The CMU walls with the CFRP and Kevlar retrofit saw the highest peak deflection values and the lowest total percent improvement. Even though these two materials did not increase the wall's strength as greatly as the metals, they still provided a significant decrease in peak deflection when compared to the control wall. On top of improving the control CMU wall, the FRP material is a much easier and workable method in terms of retrofit application. Since these two materials come as flexible sheets, this means that they can easily form around wall sections that may curve or have irregularities in shape. They can also be easily applied on-site because they do not require heavy equipment to lift, transport, or set in place. These FRPs only require the addition of heat and pressure to solidify its bond to the structure. On top of

workability, the CFRP and Kevlar is also lighter and cheaper than the aluminum and steel alternatives.

The primary objective of this investigation was to discover how each material, CFRP, Kevlar, aluminum, and steel, would perform as a retrofitting option for unreinforced CMU walls against blast loading. The secondary objective was to find the best overall retrofit option. After completing 24 runs across the four materials, the primary and secondary objectives were accomplished, and the following shows a summary of the conclusions that were found.

1. CFRP improved the wall deflections 29% to 68% when compared to the control.
2. Kevlar improved the wall deflections by 34% to 65% when compared to the control.
3. Aluminum improved the wall deflections by 25% to 69% when compared to the control.
4. Mild steel improved the wall deflections by 37% to 79% when compared to the control.
5. Mild steel performed the best in overall terms of deflection.
6. CFRP and Kevlar performed well under blasts and would be the best overall option for retrofitting unreinforced masonry.

5.2 RECOMMENDATIONS FOR FUTURE WORK

The following list is a set of recommendations to be done for future work.

1. Investigate the effect of different charge weights and standoff distances.
2. Investigate the use of other available fiber reinforced material such as GFRP and spray-on polymers.
3. Investigate the effect of different epoxy resin strengths and methods of application.
4. Investigate the use of using reinforcement strips instead of sheets and panels.
5. Investigate the combination of using two different materials in the same retrofit design (e.g., aluminum and carbon fiber).
6. Investigate how the temperature increase created by the blast affects the material strengths at short standoff distances.

REFERENCES

- [1] Federal Bureau of Investigation. “Oklahoma City Bombing.” *FBI: Federal Bureau of Investigation*, <https://www.fbi.gov/history/famous-cases/oklahoma-city-bombing>.
- [2] CNN. “Norway Terror Attacks Fast Facts.” Cable News Network, 2020, <https://www.cnn.com/2013/09/26/world/europe/norway-terror-attacks/index.html>.
- [3] History. “Boston Marathon Bombing.” A&E Television Networks, LLC., March 2014, <https://www.history.com/topics/21st-century/boston-marathon-bombings>.
- [4] BBC News. “Beirut explosion: What we know so far.” BBC, August 2020, <https://www.bbc.com/news/world-middle-east-53668493>.
- [5] Mamlouk, Michael S., and John P. Zaniewski. *Materials for Civil and Construction Engineers*. 3 ed., Pearson, 2010.
- [6] ElSayed, M., and W. W. El-Dakhakhni. “Masonry Design for Blast Loading.” *15th International Brick and Block Masonry Conference*, 2012, p. 11.
- [7] Buchan, P. A., and J. F. Chen. “Blast resistance of FRP composites and polymer strengthened concrete and masonry structures - A state-of-the-art review.” *ScienceDirect*, 2007, p. 14.
- [8] Urgessa, Girum S., and Arup K. Maji. “Dynamic Response of Retrofitted Masonry Walls for Blast Loading.” *Journal of Engineering Mechanics*, 2010, p. 7.
- [9] Pereira, João M., et al. “Masonry Infill Walls Under Blast Loading Using Confined Underwater Blast Wave Generators (WBWG).” *8th International Conference AMCM 2014*, 2014, p. 10.
- [10] Federal Emergency Management Agency (FEMA). *Unreinforced Masonry Buildings and Earthquakes: Developing Successful Risk Reduction Programs*. FEMA, 2009.
- [11] National Concrete Masonry Association. “Design of Concrete Masonry Walls for Blast Loading.” *CMA TEK 14-21A*, 2014, p. 9.
- [12] American Society of Civil Engineers. *Blast Protection of Buildings (ASCE/SEI 59-11)*. American Society of Civil Engineers, 2011.

- [13] Oesterle, Michael G., et al. "Response of Concrete Masonry Walls to Simulated Blast Loads." *Structures 2009: Don't Mess with Structural Engineers 2009 ASCE*, 2009, p. 10.
- [14] Masonry Standards Joint Committee (MSJC). *Building Code Requirements and Specification for Masonry Structures (TMS 402-13/602-13)*. Longmont, CO, The Masonry Society, 2013.
- [15] International Masonry Institute. "02.410.0131: Low Lift Grouting Procedures." *Masonry Detailing Series*, 2011, <https://www.imiweb.org/02-410-012-horizontal-joint-reinforcement-tolerance/>.
- [16] Tanner, Jennifer E., and Richard E. Klingner. *Masonry Structural Design*. Second ed., McGraw-Hill Professional, 2017.
- [17] Baxani, Mayur, et al. "Analysis of Masonry Wall Under Blast Loads Using Coupled Lagrangian-Eulerian Method." *International Conference of Advances in Civil Engineering Material and Processes (ICACEMAP)*, 2015, p. 9.
- [18] Alkhrdaji, Ph.D., P.E., Tarek. "Strengthening of Concrete Structures Using FRP Composites." *STRUCTURE Magazine*, 2015.
- [19] ISIS Education Committee. "ISIS Education Module No. 3: An Introduction to FRP-Reinforced Concrete." *ISIS Canada*, 2006, p. 35.
- [20] Karataş, Meltem A., and Hasan Gökçaya. "A Review of Machinability of Carbon Fiber Reinforced Polymer (CFRP) and Glass Fiber Reinforced Polymer (GFRP) Composite Materials." *Defence Technology*, vol. 14, no. 4, 2018, pp. 318-326. *ScienceDirect*.
- [21] Grace, Nabil F., et al. "Strengthening of Concrete Beams Using Innovative Ductile Fiber-Reinforced Polymer Fabric." *ACI Structural Journal*, no. September-October 2002, 2002, p. 9.
- [22] Ye, J. Q. "Interfacial Shear Transfer of RC Beams Strengthened by Condensed Composite Plates." *Cement & Concrete Composites*, 2001.
- [23] Prince-Lund Engineering, PLC. "FRP Reinforcement for Structures." *Prince-Lund Engineering, PLC: Inclusive Engineering*, <https://www.princelund.com/frp-reinforcement.html>. Accessed November 2019.

- [24] Fibre Glast Developments Corp. "Prepreg Fabrics." *FIBREGLAST*, 2020, https://www.fibreglast.com/category/PrePreg_Fabrics.
- [25] Bin Kabir, Reashad, and Nasrin Ferdous. "Kevlar - The Super Tough Fiber." *International Journal of Textile Science*, 2012, pp. 78-83. *Scientific & Academic Publishing*.
- [26] DuPont. "Kevlar." *DuPont*, <https://www.dupont.com/brands/kevlar.html>.
- [27] World Steel Association. "Steel in Buildings and Infrastructure." *worldsteel Association*, 2020, <https://www.worldsteel.org/steel-by-topic/steel-markets/buildings-and-infrastructure.html>.
- [28] National Concrete Masonry Association. "Steel Reinforcement for Concrete Masonry." *TEK 12-04D*.
- [29] thyssenkrupp Materials (UK). "Uses of Aluminum." *thyssenkrupp: engineering.tomorrow.together*, 2018, <https://www.thyssenkrupp-materials.co.uk/uses-of-aluminium.html>.
- [30] Abou-Zeid, B. M., et al. "Response of Arching Unreinforced Masonry Walls to Blast Loading." *11th Canadian Masonry Symposium*, 2009.
- [31] ANSYS, Inc. *AUTODYN User Manual Version 12.1*. ANSYS, Inc., 2009.
- [32] United Nations. "Kingery-Bulmash Blast Parameter Calculator." *UN SaferGuard: International Ammunition Technical Guidelines*, <https://www.un.org/disarmament/un-saferguard/kingery-bulmash/>.
- [33] Steel Forge. "AISI / SAE 4340 Alloy Steel." *All Metals & Forge Group*, L. A. Weiss, 2020, <https://www.steelforge.com/alloy-steel-4340/>.
- [34] Master Bond. "Epoxy Systems." *Master Bond: Adhesives, sealants, coatings*, <https://www.masterbond.com/products/epoxy-systems>.
- [35] Seyedrezai, Seyedehshadi. *Modeling of Arching Unreinforced Masonry Walls Subjected to Blast Loading*. McMaster University, 2011.
- [36] Musynski, Larry C., and Michael R. Purcell. "Use of Composite Reinforcement to Strengthen Concrete and Air-Entrained Concrete Masonry Walls against Air Blast." *Journal of Composites for Construction*, 2003.

- [37] Fibre Glast Distribution Corp. “Prepreg 3K, 2x2 Twill Weave Carbon.” *FIBREGLAST*,
https://www.fibreglast.com/product/Prepreg_3K_2x2_Twill_Weave_Carbon_03101.
- [38] Fibre Glast Distribution Corp. “KEVLAR Plain Weave Fabric.” *FIBREGLAST*,
https://www.fibreglast.com/product/Kevlar_Plain_Weave_Fabric_2469/Kevlar.
- [39] Fibre Glast Distribution Corp. “System 2000 Laminating Epoxy Resin.” *FIBREGLAST*, 2020,
https://www.fibreglast.com/product/System_2000_Epoxy_Resin_2000
- [40] MetalMiner. “Aluminum: MetalMiner Prices.” *MetalMiner*,
<https://agmetalminer.com/metal-prices/aluminum/>
- [41] MetalMiner. “Carbon Steel: MetalMiner Prices.” *MetalMiner*, 2020,
<https://agmetalminer.com/metal-prices/carbon-steel/>.
- [42] Ehsani, Mo, and Carlos Pena. “Blast Loading Retrofit of Unreinforced Masonry Walls With Carbon Fiber Reinforced Polymer (CFRP) Fabrics.” *STRUCTURE Magazine*, 2009.

